Helsinki University of Technology
Laboratory of Computational Engineering
Espoo 2006

REPORT B60

COMPUTATIONAL STUDIES OF SILICON INTERFACES AND AMORPHOUS SILICA

Sebastian von Alfthan

Dissertation for the degree of Doctor of Science in Technology to be presented with due permission of the Department of Electrical and Communications Engineering, Helsinki University of Technology, for public examination and debate in Auditorium N at Helsinki University of Technology (Espoo, Finland) on the 18th of December, 2006, at 12 noon.

Helsinki University of Technology
Department of Electrical and Communications Engineering
Laboratory of Computational Engineering

Tekniska Högskolan
Avdelningen för el och telekommunikationsteknik
Laboratoriet för datorbaserad vetenskap och teknik

Teknillinen korkeakoulu
Sähkö- ja tietoliikennetekniikan osasto
Laskennallisen tekniikan laboratorio

Distribution:
Helsinki University of Technology
Laboratory of Computational Engineering
P. O. Box 9203
FIN-02015 HUT
FINLAND
Tel. +358-9-451 4845
Fax. +358-9-451 4830
http://www.lce.hut.fi

Online in PDF format: http://lib.tkk.fi/Diss/2006/isbn9512285401/

E-mail: Sebastian.von.Alfthan@iki.fi

ISBN-13 978-951-22-8539-6 (printed)
ISBN-10 951-22-8539-8 (printed)
ISBN-13 978-951-22-8540-2 (PDF)
ISBN-10 951-22-8540-1 (Pdf)
ISSN 1455-0474

Picaset Oy
Helsinki 2006

Abstract

Computational simulations are a new branch of science where one can perform computational experiments by simulating a model system. The model contains an approximation of a real system with simplified physical laws and reduced size in order to make it computationally tractable. Many physical systems cannot be analytically solved and also experimentally not everything can be measured. Computational simulations fill the gaps and allow new kinds of problems to be addressed.

Two main issues are studied in this thesis with computational simulations. The first issue concerns interfaces in silicon and is studied with deterministic molecular dynamics simulations. The second issue concerns the amorphous state of silicon and silica created with a stochastic algorithm.

As for the first issue the first study is a preliminary investigation of the heat conductivity over an amorphous-crystalline interface in silicon. Second, we present a methodology for calculating the life-time of large amorphous clusters embedded in a crystalline matrix by simulating much smaller clusters. We employ this methodology to study amorphous silicon clusters and find that the activation energy of the boundary movement is temperature dependent with a change in behavior at 1150 K. The last problem concerns the structure of twist grain boundaries at 0 K. We present detailed simulations where we explore many possible grain boundary structures by allowing the number of atoms at the interface to change. This is a degree of freedom that has not been previously considered in computational studies and proved to be of utmost importance. We find that the twist grain boundaries have ordered structures at 0 K for atomic densities at the interface not previously considered. We also find that the structural unit model is valid for twist grain boundaries and present the structural units forming the boundary.

The second issue concerns the amorphous state of silicon and silica. With a stochastic Monte Carlo simulation method that operates on the bond network of silicon and silica, we have created both amorphous silicon and silica. We find that we can improve the structural description of amorhous silica by adjusting the potential model. In addition, we developed optimizations for the simulation method which made it tractable for larger systems.

Sammandrag

Simulationer utförda med datorer är en ny vetenskapsgren, där man kan genomföra datorexperiment genom att simulera ett modellsystem. Modellen innehåller en approximation av ett verkligt system med förenklade fysikaliska lagar och förminskad storlek. Många fysikaliska system kan inte lösas analytiskt, och även experimentellt går det inte att mäta allting. Simulationer fyller i luckorna och möjliggör forskning inom nya områden.

Två huvudsakliga frågor har undersökts med simulationer i denna avhandling. Den första frågan gällande gränssnitt i kisel undersöks med hjälp av deterministiska molekylärdynamik-simulationer. Den andra frågan gäller det amorfa tillståndet i kisel samt kiseldioxid, och undersöks med hjälp av en stokastisk algoritm.

Den första studien är en preliminär undersökning av värmeledningsförmågan genom ett gränssnitt mellan amorft och kristallint kisel. Den andra studien presenterar en metodologi med vilken man kan beräkna livslängden för stora amorfa klot inbyggda i en kristall genom att simulera små klot. Vi använder oss av denna metodologi för att studera amorfa kiselklot, och finner att gränssnittets rörlighet har en temperaturberoende aktiveringsenergi. Den sista studien i den första frågan gäller den atomistiska strukturen av korngränser vid 0 K. Vi presenterar detaljerade simulationer, i vilka vi undersöker flera olika korngränsstrukturer genom att variera mängden atomer vid kontaktytan. Detta är en frihetsgrad som inte har tidigare beaktats, och den visade sig vara mycket betydelsefull. Vi kommer fram till att korngränser har en ordnad struktur, samt att korngränser är uppbyggda av strukturella enheter.

Den andra frågan gäller det amorfa tillståndet av kisel samt kiseldioxid. Vi har skapat amorft kisel och kiseldioxid med hjälp av en stokastisk Monte Carlometod som opererar på nätverket av atombindningar. Vi har kommit fram till att vi kan förbättra den strukturella beskrivningen av amorft kiseldioxid genom att modifiera dess potentialmodell. Vi har även utvecklat en optimerad version av metoden, vilket möjliggör simuleringar av större system.

Preface

The research presented in this dissertation has been carried out at the Laboratory of Computational Engineering at Helsinki University of Technology during the years 2002-2006. First, I would like to thank Prof. Adrian Sutton for his guidance, and for being a great source of inspiration. His knowledge and ideas have been of vital importance in my research. I would also like to express my gratitude to Prof. Kimmo Kaski for support and for providing excellent facilities at the laboratory. Dr. Antti Kuronen was of great help in the first part of this study. In addition, I would like to thank Fred Streitz and Jim Glosli for hosting me at Lawrence Livermore National Laboratory in the summer of 2005, which was a great experience both professionally and personally.

I am also thankfull to past and present colleagues and friends at the laboratory, especially Teemu Leppänen, Markus Miettinen, Petri Nikunen, Laura Kauhanen, Ilkka Kalliomäki, Toni Tamminen and Aapo Nummenmaa. In addition, I would like to thank my family for getting me this far. Finally, I would like to thank Virpi for all the support she has given.

Sebastian von Alfthan

List of publications and author's contributions

This dissertation consists of an overview and the following publications:

I. S. von Alfthan, A. Kuronen, K. Kaski, *Crystalline-amorphous interface: molecular dynamics simulation of thermal conductivity*, Mater. Res. Soc. Symp. Proc. **703**, V6.2.1 (2002).

II. S. von Alfthan, A. Kuronen, K. Kaski, *Realistic models of amorphous silica: A comparative study of different potentials*, Phys. Rev. B **68**, 73203 (2003).

III. S. von Alfthan, A.P. Sutton, A. Kuronen, K. Kaski, *Stability and crystallization of amorphous clusters in crystalline Si*, J. Phys.: Condens. Matter **17**, 4263 (2005).

IV. S. von Alfthan, P.D. Haynes, K. Kaski, A.P. Sutton, *Are the structures of twist grain boundaries ordered at 0 K*, Phys. Rev. Lett. **96**, 55505 (2006).

V. S. von Alfthan, K. Kaski, A.P. Sutton, *Order and structural units in simulations of twist grain boundaries in silicon at absolute zero*, Phys. Rev. B **74**, 134101 (2006).

In the overview, these publications are referred to by their roman numerals. The author has played an active and vital role in the research reported here. He has performed all computational simulations and written the simulation programs, with two exceptions: the molecular dynamics program used in Publications I and III and the DFT simulations in Publication IV. He has also analyzed the simulation data and has developed all non-standard analysis tools. In addition, he has developed a visualization software which has been used for figures in Publications III-V. The author has written Publications II-V and has contributed to writing Publication I.

Contents

Chapter 1

Introduction

In physics there has traditionally been two branches of research, theoretical and experimental. Theories describe our understanding of the laws of nature, and experiments attempt to measure physical phenomena. Theories are tested and verified by experiments, while new insights for theories are gained from experiments. In addition to physical experiments there are now also computer simulations which are in some sense computational experiments. Experiments and simulations are often able to measure different things in a system and so a more complete understanding can be obtained by combining both approaches. Even fairly simple systems are often not analytically solvable though all laws governing its behavior are known. For example, Newton's laws of motion cannot be solved analytically for more than two interacting bodies. With simulations one can only obtain approximate solutions to such problems.

In computer simulations the structure and physics of a system is modeled and a computational system is constructed. In atomistic simulations the movement of atoms is simulated either with a stochastic Monte Carlo (MC) simulation, or with a deterministic molecular dynamics (MD) simulation where Newton's equations of motions are iteratively solved. Various measurements can then be carried out on the simulated systems. There are two principal limitations for computer simulations. First, the computational models are only approximations of real physical systems for the models to be computationally tractable. In analyzing simulation results care has to be taken to estimate the errors these approximations give rise to. Second, both the length and time scales are limited due to limited computational resources. However, due to technological advances the amount of computational resources grows with a rapid pace allowing more realistic models to be used, and larger length and longer time scales to be simulated.

Computer simulations are one of the oldest applications for computers (Frenkel et al., 2001). During and after the Second World War the first general purpose computers had been developed for developing nuclear weapons and to break en-

cryptions. In the beginning of the 1950s computers became available for non-military applications. Some of the first computer simulations were stochastic simulations of dense liquids. These were carried out in 1953 by Metropolis, Rosenbluth, Teller and Teller (Metropolis et al., 1953) with the Metropolis Monte Carlo method which is still in use today. The first deterministic molecular dynamics simulations were performed on a real system in 1959 (Gibson et al., 1960) when radiation damage in Cu was studied.

In this work structures in two materials, silicon and silicon dioxide (silica), have been studied. Silicon is perhaps the most common material for integrated circuits (ICs). Modern electronic devices use a wide variety of ICs, everything from micro processors in computers to embedded chips in kitchen appliances. These ICs are manufactured by forming functional units on top of a silicon substrate. By masking parts of the substrate, one can selectively dope the substrate with other elements, changing the electric properties of the unmasked areas. Also, by oxidizing unmasked areas one can create patches with amorphous silica acting as an insulator. The functional structures in devices have ever diminishing size as more and more features are packed in each chip. The feature size is now of the order of tens of nanometers. The atomistic structure of the material is of increasing interest as the size approaches the atomistic limit. Also, the continuum properties of materials are ultimately dependent on the atomistic scale properties.

This thesis is written as a compilation of five scientific Publications included in chronological order focusing on two main research issues. The first issue is explored in Publications I and III-V and it studies interfaces in silicon using deterministic molecular dynamics simulations. In Publication I heat transfer over an interface between amorphous and crystalline silicon is studied. Publication III discusses the stability of spherical clusters of amorphous silicon embedded in crystalline silicon. Publications IV and V present a new method for finding 0 K twist grain boundary structures. The second issue consists of Publication II and it covers the development of a potential model for stochastic Monte Carlo simulations of amorphous silica.

The first four chapters of the thesis give background information on the research presented in the Publications. In Chapter 2 the studied materials and structures are briefly discussed. Chapter 3 discusses computational simulation methods in some detail while Chapter 4 discusses computational methods for analyzing the simulations. In Chapter 5 we give a short summary of the results of the Publications. Finally, in Appendix A we give an introduction to the visualization software that we have developed.

Chapter 2

Interfaces and disorder in silicon and silica

In this thesis systems of silicon dioxide (silica) and pure silicon (Si) have been studied. In the case of silica an improved computational method for creating amorphous silica has been developed. In the case of Si systems, interfaces between amorphous and crystalline Si have been studied. In addition, the structure of twist grain boundaries has been explored in detail.

The chapter is organized as follows. Si and silica are first discussed. The structure and thermodynamic properties of the amorphous state are then discussed. Finally grain boundaries in Si are presented.

2.1 Silicon

Si is an element of the IV:th group in the periodic table. In its pure crystalline form, it is a hard and brittle material and dark grey in color. In nature Si does not exist on its own, but is part of minerals such as silica and silicates, which are compounds of Si with oxygen and metals. It is one of the most abundant element in the crust of the earth, a quarter of its mass being in the form of Si. At room temperature and normal pressure pure Si in its stable form is crystalline with a diamond lattice structure (Fig. 2.1). The diamond lattice can be constructed as two overlapping face centered cubic lattices, which have been displaced along the diagonal of the cube by one fourth of the length of the diagonal. Each Si atom is connected to four other Si atoms by covalent bonds so that the neighboring atoms form the vertexes in a tetrahedron. The average angle between each bond to an atom is $\cos(1/3) \approx 109.47^\circ$ and the average length of a bond is 2.35 Å at 0 K.

Si is a semiconductor and forms the basis for the majority of semiconductor components. This is because it has a number of useful properties. First, it is possible to grow large crystals of pure Si with a very low density of defects. The

largest substrates used in industrial production have a diameter of 300 mm and the density of uncontrollable impurities is of the order of 10^{13} cm^{-3} with the number of atoms being of the order of 10^{26} cm^{-3}. Second, Si has a band gap of 1.12 eV and remains a semiconductor at temperatures useful for semiconductor devices. The conductivity of Si can be easily controlled by doping the material. The band gap of Si is not direct, which means that it is optically inactive. In optical devices such as lasers one has to use materials which have a direct band gap, for example GaAs. Third, Si oxidizes easily and forms a dielectric insulator.

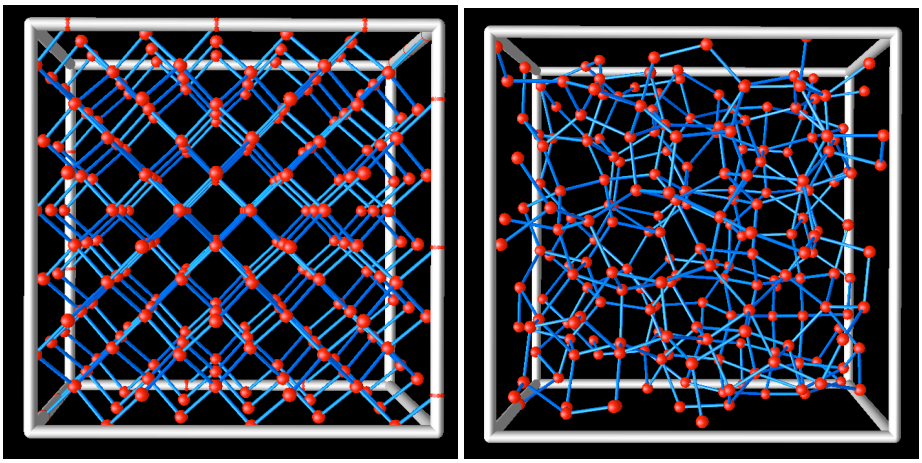

Figure 2.1: Si in two different states is illustrated. The white bars denote the supercells. Bonds which extend over periodic boundaries are not shown. *Left:* Crystalline Si. *Right:* Amorphous Si.

2.2 Silica

Silica or silicon dioxide (SiO_2) exists in the amorphous state (Fig. 2.2) as well as in a variety of different crystalline forms, i.e. polymorphs. In the literature as many as 40 different polymorphs have been described but only eight of them are of pure SiO_2 (Keskar and Chelikowsky, 1992). Of these eight polymorphs, only six have a stable structure. The eight polymorphs are α-quartz, β-quartz, α-tridymite, β-tridymite, α-cristobalite, β-cristobalite, coesite and stishovite. Of these the unstable polymorphs are the α-forms of tridymite and cristobalite. The phase diagram of silica is presented in Fig. 2.3. All these polymorphs except stishovite are formed of corner sharing $Si(O_{1/2})_4$ tetrahedrons. Corner sharing means that two neighboring tetrahedrons are connected to each other by having a common oxygen atom. Thus all oxygen atoms are members of two different

tetrahedrons and there are no Si-Si or O-O bonds. Stishovite is a high density form of silica with a much higher density than the rest of the polymorphs and it is formed of distorted $Si(O_{1/3})_6$ octahedrons sharing edges and corners.

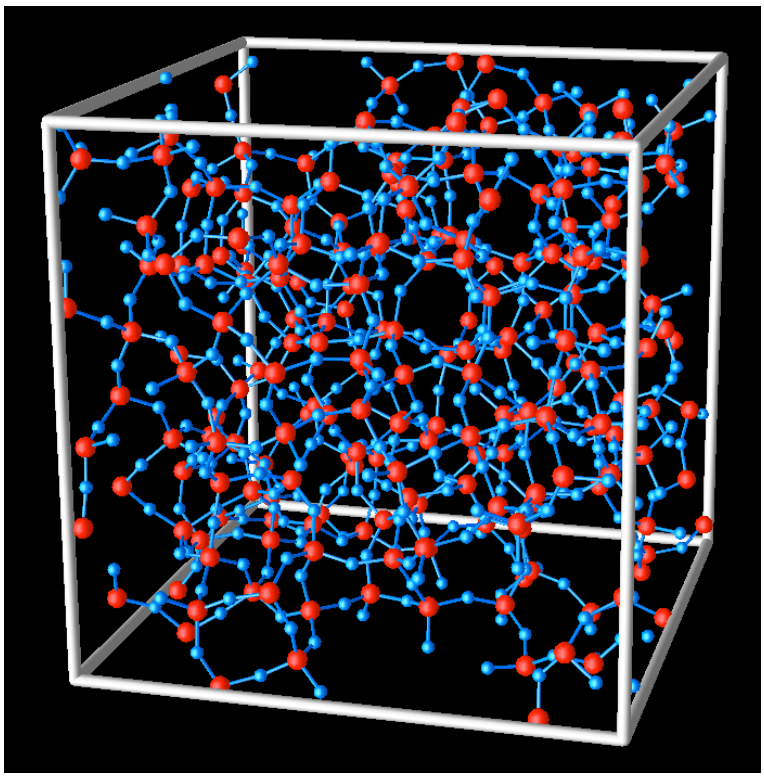

Figure 2.2: An illustration of amorphous silica. The white bars denote the supercell. Bonds which extend over periodic boundaries are not shown. Red atoms are Si atoms and blue atoms are oxygen atoms.

2.3 Amorphous state

A crystalline solid is characterized by having a periodic, ordered structure. In contrast, the amorphous phase is disordered (Fig. 2.1) and while it usually has some short-range order there is no long-range order (Morigaki, 1999). A common amorphous solid in everyday life is window glass, the main constituent being silica. In amorphous Si and silica the local environment is similar to the one in the crystalline phase. The difference is that the tetrahedrons formed by each Si atom are connected to each other in a random fashion. The amorphous state is metastable, since the free energy of the crystalline state is lower.

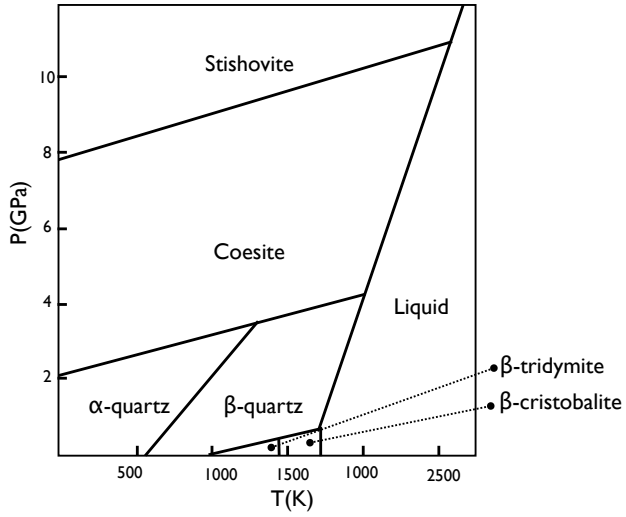

Figure 2.3: The phase diagram of silica.

Glasses are a category of amorphous solids which are characterized by having a glass transition. Structurally they are viewed as a frozen liquid while rheologically they are solid, i.e. they do not flow. When a glass forming material in its liquid state is annealed with a high enough rate, it does not crystallize and forms supercooled liquid. Upon further annealing the supercooled liquid undergoes a glass transition at temperature T_g. The glass transition is not a normal phase transition in that there is no well defined transition temperature. The faster the cooling, the higher T_g is. If the annealing is slow enough, the material will crystallize and does not undergo a glass transition.

It is widely believed that amorphous Si is not a glass forming material as the structure of liquid and amorphous Si is different. The normal liquid state of Si has an average coordination number of 6 and a density of 2.55 g/cm^{-3}, while amorphous Si has a average coordination number of 4 and a density of 2.29 g/cm^{-3}. As the quenching rates required to form amorphous Si are very high (of the order of 10^9 Ks^{-1}) it is hard to measure the phase transition from a liquid to an amorphous state. Recently it has been suggested (Hedler et al., 2004) that amorphous Si can form in a glass transition at 1000 K from a low density liquid with an average coordination of 4.

2.4 Grain boundaries in silicon

A grain boundary (GB) is an interface between two crystalline grains which destroys the translational symmetry of the grains (Howe, 1997). Heterophase GBs are formed between two grains of different composition while homophase GBs are formed between grains of identical composition. In the case of homophase GBs the two grains can differ from each other in at least two ways, i.e. by having different orientation or by having a stacking fault. Stacking faults are formed when the entire atomic layer is removed from a single crystal.

This work focuses on GBs formed between Si grains with a misorientation between them. These kinds of interfaces exist in polycrystalline Si and have a large influence on their macroscopic properties such as electronic (Grovenor, 1985) and mechanical properties. Electronic properties that are affected are conduction and the addition of charge-trapping states at the GBs. Among the affected mechanical properties are compatibility stresses caused by heating or external stress. The GBs can also be a sink for lattice dislocations. In addition, they can act as a barrier to plastic deformation by inhibiting dislocation slip and by changing the creep characteristics (Sutton and Balluffi, 1995). Polycrystalline Si is used in solar cells, thin film transistors (TFTs) in flat-panel liquid-crystal displays (Brotherton, 1995) and in solid-state image sensors. In TFTs the channel comprises polycrystalline Si which is manufactured by low-pressure chemical vapor deposition of Si on a SiO_2 substrate. The properties of polycrystalline Si are to a large degree dependent on the microscopic structure of the GBs. In this work an attempt has been made to answer some question regarding the atomistic structure of GBs.

2.4.1 Geometry

An arbitrary GB can be thought to have formed out of a single crystal by cleaving it along a plane into two grains, A and B. This plane is defined by its normal **n**. After cleaving, the B grain is rotated by an angle θ around a rotation axis **l**. Where the A and B grains intersect, the atoms belonging to the B grain are removed and voids are filled by extending the B grain. Now an arbitrary GB has been formed with five macroscopic degrees of freedom, such that three of them describe the misorientation of the two grains while two describe the lattice plane of the GB. There are two groups of GBs which have a special relationship between **n** and **l**. In tilt GBs **n** and **l** are perpendicular to each other which means that the rotation axis lies in the same plane as the GB. A special case of tilt GBs are symmetric tilt boundaries in which both grains have been rotated symmetrically so that the boundary plane is equivalent in both grains. This is perhaps the best researched GB as it is simple to study both experimentally and computationally. In twist GBs **n** and **l** are parallel to each other. All other boundaries are general boundaries and have both tilt and twist characteristics. In addition to the five

macroscopic degrees of freedom the boundary also has microscopic degrees of freedom, which include the translation of the two grains with respect to each other and the atomistic structure at the interface.

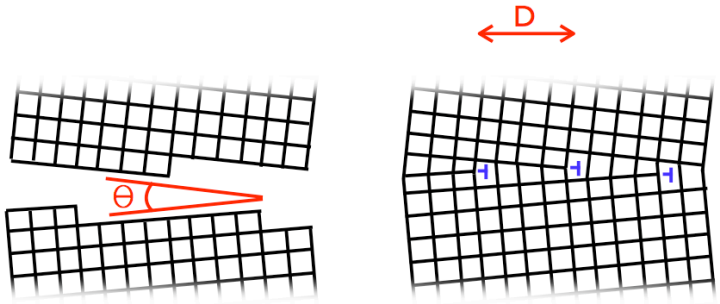

Figure 2.4: An illustration of the formation of a symmetrical tilt grain boundary. The steps on the free surfaces in the illustration on the left-hand side become edge dislocations (marked with blue) in the illustration on the right-hand side. The misorientation θ and the distance D between dislocations are also shown in red.

The structure of low angle GBs consist of dislocations where the misorientation is relieved, separated by patches of perfect crystal. In the case of pure tilt GBs, these dislocations are edge dislocations where the line of the dislocation lies in the boundary plane (Fig. 2.4). In the case of twist boundaries a network of screw dislocations is formed (Fig. 2.5). The distance D between the dislocations in a symmetrical low angle tilt GB is given by

$$D = \frac{b}{2\sin(\theta/2)} \approx \frac{b}{\theta}, \tag{2.1}$$

where b is the length of the Burgers vector of a dislocation and the approximation is valid for small θ. The distance between the screw dislocations in twist GBs is also given by Eq. 2.1. The energy per unit area γ_{GB} of such a boundary has been calculated analytically by Read and Shockley (1950) and is given by

$$\begin{aligned} \gamma_{GB} &= E_0\theta(A_0 - \ln\theta), \\ E_0 &= \frac{\mu b}{4\pi(1-\nu)}, \\ A_0 &= 1 + \ln\left(\frac{b}{2\pi r_0}\right), \end{aligned} \tag{2.2}$$

where μ is the shear modulus, ν is the Poisson's ratio and r_0 is the core energy of a single dislocation. The A_0 term models the core energy of the dislocations while

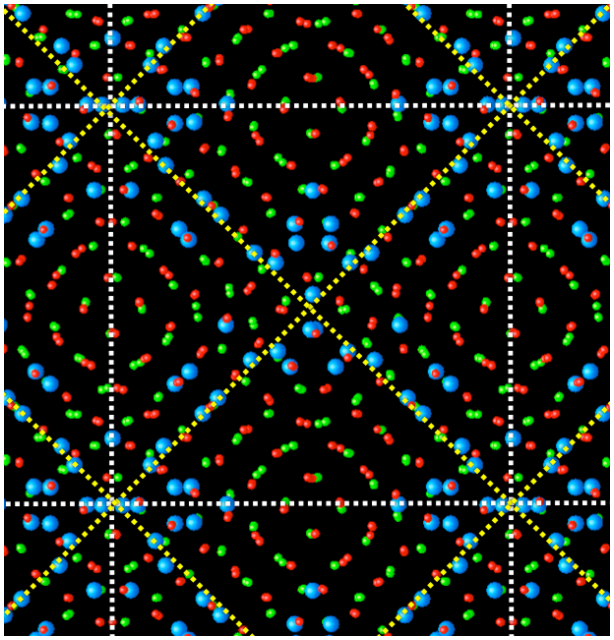

Figure 2.5: A plane view of a relaxed low-angle twist GB in silicon. The large blue atoms are in the GB, red atoms are in the upper crystal grain and green atoms are in the lower one. A screw dislocation network denoted by yellow dashed lines is seen, separated by patches of crystalline grains. The periodic unit cell is denoted by dashed white lines.

the $\ln\theta$ term models the elastic energy. For asymmetrical tilt GBs there are two sets of edge dislocations with extra planes that are perpendicular to each other, and Eq. 2.2 can be generalized to give the energy of such a boundary. As the misorientation angle increases, the dislocation separation decreases and the Read and Shockley description, being based on isolated dislocations, breaks down. Both tilt and twist GBs exhibit cusps in the energy at certain misorientations for which lattice points of grains A and B coincide (Fig. 2.6). The lattice formed by these coincident points is the coincident site lattice (CSL). For each CSL there is a characteristic Σ value, which stands for the inverse density of coincident sites. In Fig. 2.7 the $\Sigma 5$ twist grain boundary in Si is viewed along the boundary normal [001] and every fifth atom is a coincident site in each grain. The CSL cell edges are given by the 1/2<210> vectors. In a cubic lattice such as Si the Σ value can be calculated with the following equation if the boundary has been rotated along $< 100 >$, i.e.

$$\Sigma = x^2 + y^2, \tag{2.3}$$

where the CSL cell edges are $< xy0 >$. If the Σ value given by the equation is

even, it must be divided by two until an odd number is obtained in order to get the true Σ value. This Σ value also corresponds to the number of atoms per CSL cell in each atomic layer parallel to the boundary.

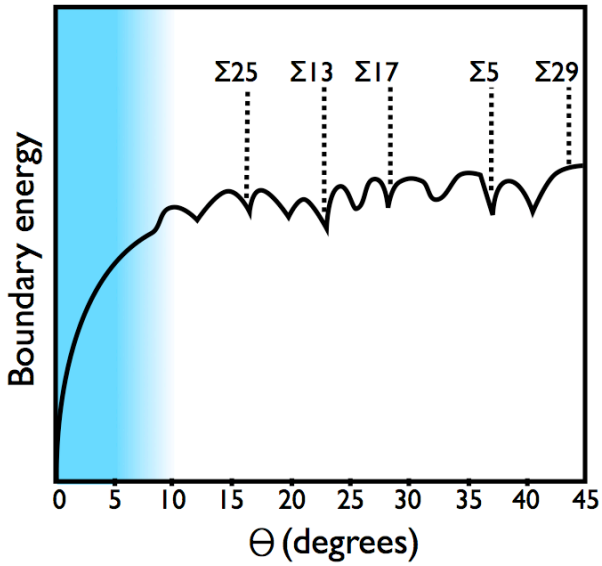

Figure 2.6: The experimentally measured GB energy (Otsuki, 2001) of a Si twist GB is sketched as a function of the misorientation angle θ. The blue shaded area shows where the Read and Shockley description (Eq. 2.2) is valid.

2.4.2 Atomistic structure

For small misorientations, where the dislocations are well separated, the atomistic structure is given by the geometrical dislocation description. As the misorientation increases, this is not true any more. For high angle GBs computer simulations and direct experimental measurements are needed to obtain the atomistic structure of the boundary. A historically contested topic has been the degree of order at the GBs (Sutton and Balluffi, 1995). They have been described both as amorphous intergranular films and as ordered boundaries. The latter picture is the one that has prevailed in the case of tilt GBs. They have been extensively studied both from experimental and computational points of view (D'Anterroches and Bourret, 1984; Kohyama et al., 1988; Sutton, 1991). It is broadly agreed that tilt GBs can be described by the structural unit model (SUM) (Sutton and Vitek, 1983). The SUM describes the boundary structure as a sequence of structural units. Each structural unit is a particular configuration of atoms, which can be linked together with other units. In addition, each boundary has a particular sequence and the structural units

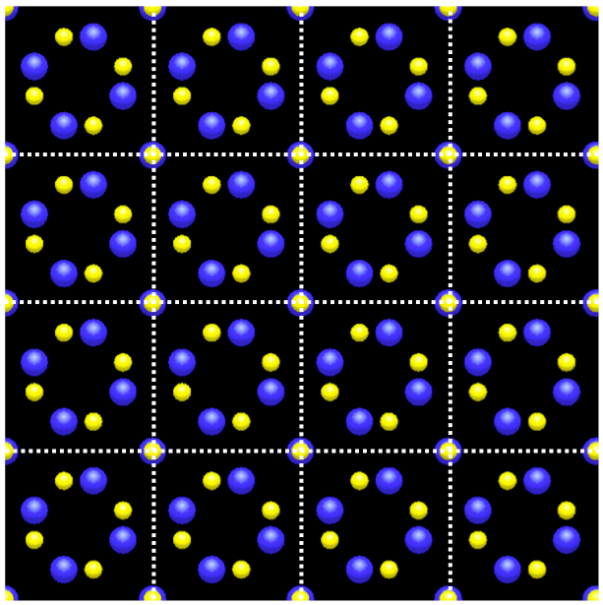

Figure 2.7: A plane view of an ideal $\Sigma 5$ twist GB. The large blue atoms belong to the grain further from the viewer and the small yellow atoms to the grain closer to the viewer. The dashed lines show the CSL.

it comprises, depend on the boundary. At misorientations between two Σ values the sequence is given by a linear mixture of the two sequences. In the case of twist GBs the results on GB structures at 0 K are less conclusive. Some earlier simulations have suggested (Keblinski et al., 1996, 1997) that high-angle twist GBs in Si lower their energies by forming disordered amorphous intergranular films even at 0 K. Other simulations of twist boundaries (Cleri et al., 1998; Tarnow et al., 1990; Payne et al., 1987; Kohyama and Yamamoto, 1994; Wang et al., 1994) did not find low energy ordered structures. However, recent experimental measurements of the energies of (001) twist GBs in Si (Otsuki, 2001) found cusps at misorientations of $\approx 16^\circ, 23^\circ, 28^\circ$ and 37°, known as $\Sigma 25$, $\Sigma 13$, $\Sigma 17$ and $\Sigma 5$ (001) twist boundaries, respectively. The measured GB energy is sketched in Fig 2.6. These observations indicate that there is some degree of structural order at the CSL misorientations. In addition to the cusps at CSL misorientations there are also cusps at intermediate misorientations. This indicates that their structure is an ordered mixture of the two neighboring CSL misorientation structures, as predicted by SUM. In Publications IV and V we have shown that the $\Sigma 25$, $\Sigma 13$, $\Sigma 17$, $\Sigma 5$ and $\Sigma 29$ boundaries have ordered, low energy structures. We have also found structural units and shown that the structures of the $\Sigma 25$, $\Sigma 13$ and $\Sigma 5$ boundaries comprise different sequences of the same two structural units.

Chapter 3

Computer simulations

In this chapter potential models describing the interaction between atoms are presented. Methods that have been used to simulate the movement of atoms are also discussed. They are divided into two categories, stochastic Monte Carlo (MC) simulations employed in Publications I and II, and deterministic molecular dynamics (MD) simulations employed in Publications I and III-V.

3.1 Potential models

In principle all interactions between atoms can be obtained by solving the Schrödinger equation (Ashcroft and Mermin, 1976) but in practice this is not possible for any system more complex than a single hydrogen atom. In order to make the problem tractable approximations have to be made. There is typically a direct correlation between the accuracy of the calculations and the system size that can be calculated. First principles, or *ab-initio* methods, are the most exact ones. They calculate the interaction of atoms by solving a simplified version of the Schrödinger equation. Perhaps the most common *ab-initio* method is the density functional method (DFT) which has been used in Publication IV to validate the results of simpler models. In the DFT method the total energy of the system is assumed to be a functional of the density of electrons. Currently, *ab-initio* methods allow the calculation of systems comprising hundreds of atoms. At the next level of approximation there are the semiempirical methods. Here even more approximations have been made to the quantum mechanical picture but on the other hand empirical parameters are employed for better description of interactions between atoms. A common semiempirical method is the tight-binding method with which systems comprising thousands of atoms can be simulated. At the lowest level of accuracy we have the empirical potential models, which allow simulations comprising even millions of atoms. Here the potential model is constructed to consist of computationally fast empirical functions. The total potential energy of the sys-

tem is assumed to be given by $E(r_1...r_N)$ which is a function of the position of all atoms. This potential can be approximated with a series,

$$E(r_1...r_N) = V_0 + \sum_i V_1(r_i) + \sum_{i,j} V_2(r_i, r_j) + \sum_{i,j,k} V_3(r_i, r_j, r_k) + ..., \quad (3.1)$$

where V_0 is simply a constant and as such does not affect the physics of the system. V_1 describes the effect of some external field and the third term, V_2, describes two-body interactions and is normally a function of the distance between a pair of atoms. The fourth term, V_3, is a three-body term which is essential in covalent materials. The first two terms in Eq. 3.1 are normally not used in computational studies. Some materials can be described with potentials containing only the two-body term. One of them is silica, for which there is both two- and three-body potential models. In contrast, Si and other materials with the diamond lattice structure cannot be described by any reasonably smooth two-body potential and a three-body part is required to stabilize the structure. The embedded atom model (EAM) potential used for metals, and the Tersoff potentials used for Si, are examples of two-body potentials with an environment dependent term in the two-body interaction giving the potential a many-body character. The functional forms can be constructed in several ways. Direct physical insight can be used to construct a potential model. An example of this is the Lennard-Jones potential which has two terms, one r^{-6} for an attractive van der Waals interaction and one r^{-12} term for short range repulsion between atoms. One can also gain insight from the solutions of the more exact methods to construct good approximations. In addition, one can construct plausible functions and find a good form based on trial and error. The parameters of the empirical potential models are either fitted to experimental data of real materials or to properties of clusters calculated using *ab-initio* methods. In this thesis only empirical potential models have been used in simulations.

For Si there are a large number of different potential models available (Balamane et al., 1992; Justo et al., 1998). Since Si is technologically very important it has been a prototype material for developing potentials for covalent materials. Also, the structural chemistry of Si is complex and the range and strength of the covalent bonding is not easily modeled by empirical models. Two popular choices for an empirical model are Stillinger-Weber (SW) (Stillinger and Weber, 1985) and Tersoff (Tersoff, 1988a). Others which can be mentioned are the Keating potential (Keating, 1966; Chan and Elliot, 1992) and the environment-dependent interatomic potential (EDIP) (Justo et al., 1998). A study comparing SW, Tersoff and some other potentials can be found at (Balamane et al., 1992), where there are also further references to other comparative studies.

Silica is also a very challenging material to model. A good interatomic potential should be able to reproduce the properties of the different polymorphs and the amorphous state. Many of the developed potentials have problems with stishovite

because it does not have the same local structure formed of tetrahedrons as the other polymorphs. It should be mentioned that silica is a very polar material in which oxygen is the negatively charged and Si is the positively charged atom. Therefore, many of the good potentials include a Coulombic interaction which is a long range interaction. This is computationally expensive and slows down the simulations. There are both two-body (Tsuneyuki et al., 1988; van Beest et al., 1990) and three-body potentials (Vashishta et al., 1990) for silica. It is perhaps a bit surprising that a two-body potential can keep the structure stable as the atomic density of silica is not very large. Because of the charge transfer from the Si atom to the oxygen atom, the oxygen atom is considerably larger than the Si atom which stabilizes the system. In this thesis a simplified Keating potential has been used because of the requirements of the simulation method. It only contains bond-bending and bond-stretching terms and it has no terms to describe long range forces.

3.1.1 Stillinger-Weber potential

The Stillinger-Weber (SW) (Stillinger and Weber, 1985) potential consists of two- and three-body terms,

$$E = \epsilon\Big[A\sum_{j>i} V_{ij} + \lambda \sum_{j\neq i, k>j} V_{ijk}\Big], \tag{3.2}$$

$$V_{ij} = \begin{cases} \Big[B\Big(\frac{r_{ij}}{\sigma}\Big)^{-p} - 1\Big]\exp\Big(\frac{1}{r_{ij}/\sigma - a}\Big), & r_{ij} < a\sigma \\ 0, & r_{ij} \geq a\sigma \end{cases} \tag{3.3}$$

$$V_{ijk} = \begin{cases} (\cos\theta_{jik} - \cos\theta_0)^2 \exp\Big(\frac{\gamma}{r_{ij}/\sigma - a} + \frac{\gamma}{r_{ik}/\sigma - a}\Big), & r_{ij}, r_{ik} < a\sigma \\ 0, & \text{otherwise} \end{cases} \tag{3.4}$$

where E is the potential energy, r_{ij} is the distance between atoms i and j and $\cos\theta_{jik}$ is the cosine of the angle between bonds ij and ik. The numerical values of the parameters are listed in Table 3.1.

The parameters of SW have been chosen to give the diamond structure as the most stable structure. In addition, they have been chosen to give both a reasonable liquid structure and the correct melting point (1687 K). Even though the parameters have not been fitted to amorphous Si, the potential is able to describe this phase reasonably well. There is also an alternative set of parameters called the 'modified Stillinger Weber potential' (MSW) (Vink et al., 2001), which has been fitted to better reproduce the amorphous state. The only difference compared to the original SW potential is that the energy of the three-body term is enhanced while the energy of the two-body term is decreased. The parameters for both SW and MSW are given in Table 3.1.

Table 3.1: Parameters for the SW and MSW potentials.

	SW	MSW
ϵ (eV)	2.16826	1.64833
A	7.049556277	7.049556277
B	0.6022245584	0.6022245584
σ (Å)	2.0951	2.0951
p	4	4
a	1.80	1.80
λ	21.0	31.5
γ	1.20	1.20
$\cos\theta_0$	-1/3	-1/3

3.1.2 Tersoff potential

The Tersoff potential is different from Stillinger-Weber and Keating in that there is no explicit 3-body term. It is defined as a sum of pair interactions where the coefficient of the attractive term depends on the local environment giving a many-body potential. The functional form is given by

$$E = \sum_i E_i = \frac{1}{2}\sum_{i\neq j} V_{ij}, \tag{3.5}$$

$$V_{ij} = f_C(r_{ij})\left[a_{ij} f_R(r_{ij}) + b_{ij} f_A(r_{ij})\right], \tag{3.6}$$

$$f_R(r) = A\exp(-\lambda_1 r), \tag{3.7}$$

$$f_A(r) = -B\exp(-\lambda_2 r), \tag{3.8}$$

$$f_c(r) = \begin{cases} 1 & r \leq R-D \\ \frac{1}{2} - \frac{1}{2}\sin\left[\frac{\pi}{2}(r-R)/D\right] & R-D < r < R+D \\ 0 & r \geq R+D \end{cases} \tag{3.9}$$

$$b_{ij} = (1+\beta^n \zeta_{ij}^n)^{-1/2n}, \tag{3.10}$$

$$\zeta_{ij} = \sum_{k\neq i,j} f_C(r_{ik}) g(\theta_{jik}) \exp\left[\lambda_3^3 (r_{ij}-r_{ik})^3\right], \tag{3.11}$$

$$g(\theta) = 1 + \frac{c^2}{d^2} - \frac{c^2}{d^2 + [h-\cos(\theta)]^2}, \tag{3.12}$$

$$a_{ij} = (1+\alpha^n \eta_{ij}^n)^{-1/2n}, \tag{3.13}$$

$$\eta_{ij} = \sum_{k\neq i,j} f_C(r_{ik}) \exp\left[\lambda_3^3 (r_{ij}-r_{ik})^3\right], \tag{3.14}$$

Table 3.2: Parameters for the Tersoff III potential.

A (eV)	1830.8
B (eV)	471.18
λ_1 (Å^{-1})	2.4799
λ_2 (Å^{-1})	1.7322
λ_3 (Å^{-1})	1.7322
R (Å)	2.85
D (Å)	0.15
α	0.0
β	1.0999×10^{-6}
n	7.7834×10^{-1}
c	1.0039×10^{5}
h	-5.9862×10^{-1}

where E is the potential energy, r_{ij} is the distance between atoms i and j and θ_{jik} is the angle between bonds ij and ik.

There are several parametrisations of the potential of which the most common is Tersoff III (Tersoff, 1988a). The parameters for this version are given in Table 3.2. These parameters have been obtained by fitting the potential to cohesive energies of different Si polytypes, the bulk modulus and bond length in the diamond structure and the three other elastic constants to within 20% of their real value. One weakness in this potential model is that it gives a melting temperature of 2550 K for Si (Cook and Clancy, 1993). The preceding parameterization (Tersoff, 1988b) has inaccurate elastic constants. It should be emphasized that the original parameterization (Tersoff, 1986) of this potential is fundamentally flawed since it predicts that the diamond structure is not the ground state.

3.1.3 Modified Keating potential

Of the potentials mentioned here the Keating potential model (Keating, 1966; Kleinman and Spitzer, 1962) is the oldest. It is a simple potential model with a bond-stretching and bond-bending term. The bond-stretching term describes the energy of bond-lengths by a spring-like term while the bond-bending term models the angle between bonds by another spring-like term. This potential has many serious shortcomings. First, its interactions do not have a natural cutoff, meaning that bonds cannot be broken. Thus it is not useful in molecular dynamics simulation as it cannot be used to simulate any structural changes. Also it is not able to reproduce all elastic constants of Si. In addition, it completely ignores the ionic character of silica and describes it as completely covalent. In the

MC method used in Publication II the Keating potential is used as the structure is evolved by directly changing the bonding network. The following version of the potential model is the one for which the author has developed a new set of parameters in Publication II. It is the so called simplified Keating potential model (Kleinman and Spitzer, 1962) which has been used for SiO_x (Tu et al., 1998; Tu and Tersoff, 2000; Burlakov et al., 2001). The modified potential has an improved description of amorphous silica in that the bond angle distribution at oxygen sites is reproduced more realistically. The functional form of the potential is given by

$$E = \sum_{j>i} V_{ij} + \sum_{m>n} R_{nm} + \sum_{j\neq i,k>j} V_{jik}, \tag{3.15}$$

$$V_{ij} = \frac{1}{2} A_{ij} \left(r_{ij} - d_{ij}\right)^2, \tag{3.16}$$

$$R_{ij} = \begin{cases} \frac{1}{2} B_{ij} \left(r_{ij}^2 - r_r^2\right)^2 & r_{ij} \leq r_r \\ 0 & r_{ij} > r_r \end{cases}, \tag{3.17}$$

$$V_{jik} = \frac{1}{2} C_{jik} \left(\cos\theta_{jik} - \cos\theta_{i,0}\right)^2, \tag{3.18}$$

where the summation of V_{ij} and V_{jik}, for each atom i, only go over those atoms which are bonded according to the explicitly defined bond network. The summation of R over m and n only go over those atoms which are neither nearest nor second nearest neighbors. This term adds repulsion between non-bonded atoms and is required to avoid atoms overlapping during minimization. This helps the minimization to avoid getting trapped in unphysical metastable states. In the final minimized structure this potential energy term should not contribute to the energy. r_{ij} is the distance between atoms i and j and $\cos\theta_{jik}$ is the cosine of the angle between bonds ij and ik. d_{ij} is the equilibrium bond length and $\theta_{jik,0}$ is the equilibrium angle. The parameters for Si and silica developed in Publication II are given in Table 3.3.

3.2 Molecular dynamics

With the molecular dynamics (MD) method (Allen and Tildesley, 1987; Frenkel et al., 2001) both equilibrium and dynamical properties of atomistic systems can be studied. The basic idea is to perform a computational experiment by simulating the movement of atoms as a function of time. The atoms are treated classically, they are point-like and obey Newtonian mechanics. This assumption is valid for a wide range of materials and it is only at low temperatures where quantum effects start to appear. The interaction of atoms is modeled by a potential energy function which gives the forces and energies of a set of atoms. In a MD simulation the

Table 3.3: $V_{Keating}$ parameters published in Publication II.

A_{SiSi} (eV/Å^2)	9.08
A_{SiO} (eV/Å^2)	27.0
B (eV/Å^2)	0.8
C_{SiSiSi} (eV)	3.58
C_{SiOSi} (eV)	2.0
C_{OSiO} (eV)	4.32
C_{SSiO} (eV)	$\sqrt{C_{SiSiSi}C_{OSiO}}$
d_{SiSi} (Å)	2.35
d_{SiO} (Å)	1.61
r_r (Å)	2.6
$\cos\theta_{Si,0}$	-1/3
$\cos\theta_{O,0}$	-1.0

macroscopic properties of the atomistic system, such as temperature and pressure, can be measured. Also the microscopic properties are easily studied, as the position and momentum of each atom are known. Compared to real experiments, the length-scales of the system are limited by the available computational resources, at the time of writing the maximum system size is of the order of millions of atoms with a simulated time of the order of nanoseconds (Streitz et al., 2006).

3.2.1 Algorithm

Here a basic MD simulation algorithm is presented. It simulates the movement of atoms by iterating Newton's equations of motion in a fixed supercell. This means that they are in the NVE ensemble, where the number of atoms, volume and the total energy are constant. Also other ensembles can be simulated by altering the equations of motion. The pressure can be kept constant by adding a barostat and by allowing the volume to fluctuate (Berendsen et al., 1984). The temperature is kept constant by adding a thermostat and allowing the total energy to change (Nosé, 1984; Andersen, 1980; Berendsen et al., 1984).

The first step in a MD simulation is to create a starting point for the simulation. The initialization involves forming an initial atomic structure in a computational supercell and assigning initial velocities to the atoms. The initial velocities and the atomic structure give the total initial energy of the system. Usually the initial structure is a minimum energy structure such as a crystal, and all energy is inserted in the form of kinetic energy.

If the number of atoms is N then the number of atoms which are close to the edges of the supercell is proportional to $N^{-1/3}$. This means that the finite-size sur-

face effects are significant for system sizes that can be simulated. For the edges of the supercell there are two common boundary conditions, namely free and periodic boundaries. With free boundary conditions the system is surrounded by empty space which is useful for simulating surfaces and clusters. Periodic boundaries are used to simulate bulk phases that cannot be directly simulated due to limits on the number of atoms. A structure of infinite size is created by using the computational supercell as the primitive cell of a periodic lattice (Fig. 3.1). Atoms close to the boundary interact with atom images in the neighboring periodic supercell. Also, if an atom crosses the boundary its coordinates are periodically reduced so that it remains inside the computational supercell.

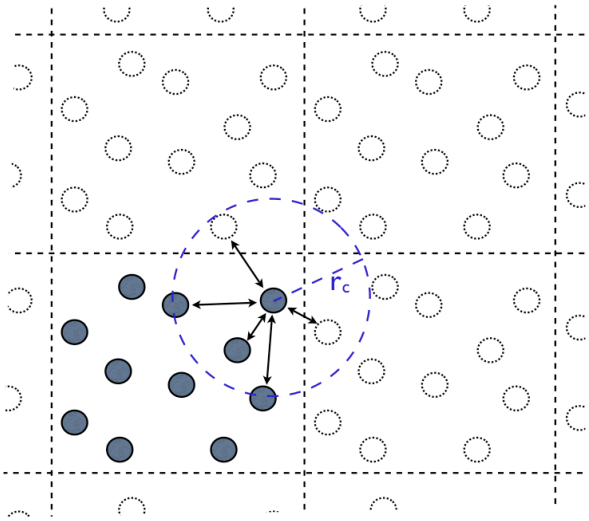

Figure 3.1: A 2D illustration of periodic boundary conditions. The lattice of supercells is marked with dashed black lines. The atoms in the computational supercell are marked by filled circles while their periodic images are marked by dashed circle lines. The atoms with which one particular atom interacts are marked by arrows. The range of the potential is marked with the blue circle, which has a radius of r_c.

After initialization the positions and velocities of the atoms are iteratively updated. The time-step of the iterative algorithm is of the order of femtoseconds so that atomic vibrations are simulated with sufficient accuracy. Perhaps the most popular algorithms are the Verlet family of algorithms where the error done during each time step is of the order of $O(\Delta t^4)$ for the positions. Other popular choices are predictor-corrector algorithms (Allen and Tildesley, 1987) which are able to simulate the movement of atoms with greater accuracy making slightly longer time steps possible. The drawback of these algorithms is that they are more complex to implement and potentially show more drift in the potential energy over

longer time scales (Frenkel et al., 2001).

The velocity Verlet algorithm in the NVE ensemble, with constant total energy and volume, reads as follows:

1. Initialize the velocity, $\mathbf{v}$, and position, $\mathbf{r}$, of each atom at time $t = 0$.
2. Update positions to time $t + \Delta t$,
$$\mathbf{r}(t + \Delta t) = \mathbf{r}(t) + \mathbf{v}(t)\Delta t + \frac{\mathbf{F}(t)}{2m}\Delta t^2. \tag{3.19}$$
3. Calculate potential energies and forces acting on atoms at time $t + \Delta t$ using the potential model. From the potential energy E, the force $\mathbf{F}$ acting on the atoms is obtained by derivation,
$$\mathbf{F} = -\nabla E. \tag{3.20}$$
4. Update velocities to time $t + \Delta t$,
$$\mathbf{v}(t + \Delta t) = \mathbf{v}(t) + \frac{\mathbf{F}(t + \Delta t) + \mathbf{F}(t)}{2m}\Delta t, \tag{3.21}$$
where m is the mass of each atom.
5. Update and output analysis data for time $t + \Delta t$
6. Update time, $t + \Delta t \rightarrow t$
7. Go to step 2 while $t < t_{max}$

3.2.2 Measured quantities

The temperature T of a simulated system is calculated from the equipartition theorem
$$\frac{3}{2}Nk_bT = E_{kin}, \tag{3.22}$$
where E_{kin} is the total kinetic energy of the system. The pressure P is calculated from the virial expansion
$$P = \frac{N}{V}k_BT + \frac{1}{dV}\left\langle \sum_{i<j} \mathbf{F}_{ij} \cdot \mathbf{r}_{ij} \right\rangle, \tag{3.23}$$
where V is the volume of the supercell, d is the dimensionality of the system and $\mathbf{F}_{ij}$ is the force acting between atoms i and j.

In this work the structure of the simulated systems has been the main point of interest and so the positions of the atoms have been written out regularly. When

analyzing the structure we are interested in the lattice points of the atoms. At elevated temperatures the atoms are vibrating around these points and so if their positions are written out at one time-step they are not in their respective lattice point. In Publications IV and V we averaged the atom positions over 300 fs before they were written out. This removed most of the thermal vibrations and allowed us to see the lattice positions also at high temperatures. In Publication III this approach would have been very useful but was not used as we had not yet adopted this approach.

3.2.3 Force calculation

In MD simulations the force acting on each atom is needed. In general the force $\mathbf{F}_i$ acting on a particle i is given by

$$\mathbf{F}_i = -\nabla_i E, \tag{3.24}$$

where E is the total potential energy of the system. It is useful to cast this equation in another form where the bond-forces are first calculated. This is both for computational convenience and for making the calculation of pressure possible. The force acting on atom i along coordinate x is

$$\begin{aligned} F_{i,x} &= -\frac{\partial E}{\partial r_{i,x}} = -\sum_j \frac{\partial E}{\partial r_{ij,x}} \frac{\partial r_{ij,x}}{\partial r_{i,x}}, \\ &= \sum_j \frac{\partial E}{\partial r_{ij,x}} = \sum_j F_{ij,x}, \\ \mathbf{F}_i &= \sum_j \mathbf{F}_{ij}, \end{aligned} \tag{3.25}$$

where $r_{i,x}$ is the x component of the position of atom i, $r_{ij,x}$ is the x component of the distance to atom j and $F_{ij,x}$ is the x component of the bond force F_{ij}. This derivation is valid since potential models are functions of the relative positions of the atoms and not absolute positions.

3.3 Monte Carlo

In MC simulations (Frenkel et al., 2001) a system is simulated via a stochastic algorithm. It can be used to do simulations both in the NVT and NPT ensembles. Also grand-canonical simulations, where the number of atoms is not constant, are possible. A typical Metropolis MC simulation of an atomic system is done as follows. The system is first prepared to some initial state. The state is then updated via a stochastic algorithm. This is done by performing a random trial step, which

changes the state to another, followed by an evaluation of the trial step where it is either rejected or accepted. There is no time scale associated with the steps, so the kinetics of the system cannot be obtained using this method but one can do measurements in the simulated ensemble. It can also be used to quench a system to a minimum energy configuration by slowly cooling it down from an initial high temperature where almost all steps are accepted.

If a system is in a NVT ensemble then the probability $p(\Gamma_i)$ that it will be in a certain state Γ_i is given by the Boltzmann distribution which reads as follows

$$p(\Gamma_i) = \frac{1}{Z(T)} \exp\left(-\frac{E(\Gamma_i)}{k_B T}\right) \tag{3.26}$$

where $E(\Gamma_i)$ is the potential energy of state Γ_i, T is the temperature, k_B is the Boltzmann constant and $Z(T)$ is the partition function:

$$Z(T) = \sum_j \exp\left(-\frac{E(\Gamma_j)}{k_B T}\right), \tag{3.27}$$

where the sum goes over all states. The basic idea in a MC simulation is to sample the state space so that the probability of being in a certain state is proportional to $p(\Gamma_i)$. The determination of $p(\Gamma_i)$ is most often done by the Metropolis algorithm which reads as follows. If α_{ij} is the probability that a trial step from state Γ_i to Γ_j is attempted, and the probability that it is accepted is p_{ij}, then the probability of moving from state Γ_i to state Γ_j is $\pi_{ij} = \alpha_{ij} p_{ij}$. In the Metropolis scheme α is assumed to be symmetric, $\alpha_{ij} = \alpha_{ji}$. This means that the probability of doing a certain trial step to a new state is equal to the probability of doing a trial step back to the original state if the new state is accepted. It is also important to assure that the system is ergodic and is thus able to visit all states of the system. If the system obeys the probability distribution of Eq. 3.26 then in equilibrium the probability distribution should be constant. This is true if the following relation is fulfilled

$$p(\Gamma_i)\pi_{ij} = p(\Gamma_j)\pi_{ji}, \tag{3.28}$$

which is the *detailed balance* condition. It tells that the probability distribution is constant since the flow in both direction is equal. By inserting $p(\Gamma_i)$ and π_{ij} and by using the symmetry of α an equation linking p_{ij} and p_{ji} is obtained, reading

$$\frac{p_{ij}}{p_{ji}} = \exp\left(-\frac{E(\Gamma_j) - E(\Gamma_i)}{k_B T}\right). \tag{3.29}$$

In the Metropolis scheme p_{ij} is chosen to be

$$p_{ij} = \begin{cases} \exp\left(-\frac{E(\Gamma_j)-E(\Gamma_i)}{k_B T}\right) & E(\Gamma_i) < E(\Gamma_j) \\ 1 & E(\Gamma_i) > E(\Gamma_j) \end{cases} \tag{3.30}$$

In simulations in the NPT ensemble one accepts the normal trial moves with the same probability as in the NVT ensemble but in addition to that, one has to make some trial moves where the volume is changed by scaling all the position coordinates in the system. These trial moves are accepted with the following probability

$$p_{ij} = min\left\{1, \exp\left(N \ln\left(\frac{V_i}{V_j}\right) - \frac{E(\Gamma_i) - E(\Gamma_j) + P(V_j - V_i)}{k_B T}\right)\right\}, \tag{3.31}$$

where V_i is the volume of state Γ_i.

3.3.1 Wooten, Winer and Weaire method

Let us now turn to a specific MC method namely the Wooten, Winer and Weaire (WWW) method which was first published in the context of creating an amorphous Si system (Wooten et al., 1985) and has later on been refined by Tu and Tersoff (2000); Burlakov et al. (2001) and Barkema and Mousseau (2000). In this work it has been used in Publications I and II to create amorphous Si and silica, respectively. It is a MC method where the state of the system is described by its network of bonds. The energy is given by the Keating potential model, which is a function of the bonding network and the position of the atoms in it. The position dependence is removed by restricting the atoms to be in their minimum energy positions with respect to the bond network. The MC moves are those that change the bond topology. In the original WWW method there is only one kind of a bond move, i.e. the bond-switch move.

In the bond-switch move two atoms exchange bonds and thus change the bond topology. It is illustrated in Fig. 3.2 for a 2D crystal where all atoms are 3-fold coordinated. The bond switch is performed by first picking one atom B at random. Then one of its neighbors is picked at random (C) and after that A, which is a neighbor of B, and D, in turn being a neighbor of C, are picked at random. By breaking the bonds AB and CD and creating bonds AC and BD a new topology is created. This works in pure Si but in SiO_x one has to adapt this move so that no O-O bonds are created as they are present only in non-equilibrium defects and are not described by the potential model. This can be done by making sure that B and C are both Si atoms separated by one oxygen atom. Such a move preserves the coordination number of all involved atoms but does change the topology. Close to the switch site the ring-statistics will change, in a perfect crystal four 6-fold rings

transform into two 5-fold rings and two 7-fold rings. After a switch is made the topology has changed, which means that the atoms are no longer in a minimum energy position. Therefore, the potential energy has to be minimized with respect to the positions of the atoms to get the true potential energy of this particular topology.

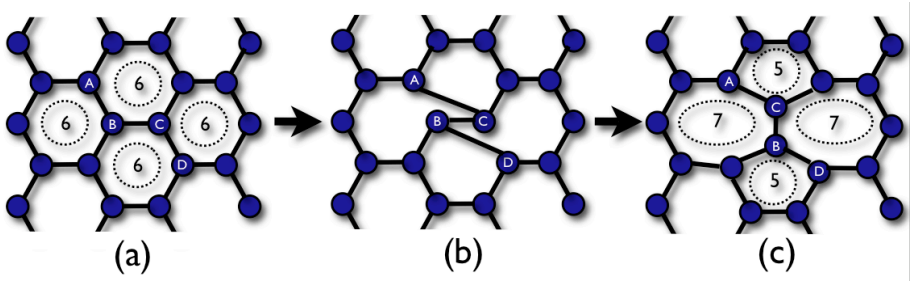

Figure 3.2: A bond-switch trial move illustrated for a 2D crystal. *a*: The initial situation with four 6-fold rings that are depicted with dashed circles. *b*: Bonds are switched so that bonds AB and CD are broken, and AC and BD are formed. *c*: The positions of the atoms have been minimized with respect to the potential energy. The four 6-fold rings have transformed into two 5-fold rings and two 7-fold rings.

One serious problem with the WWW method is that it in its original formulation scales as $O(N^2)$. The number of bonds is proportional to N and thus the number of MC moves required to evolve all parts of the system is also proportional to N. The time required to evaluate one trial step scales as $O(N)$ because of the minimization. Thus the total time required to simulate a system scales as $O(N^2)$. Barkema and Mousseau (2000) have modified the WWW algorithm so that they achieve an $O(N)$ scaling by doing local minimizations and by rejecting non-accepted steps early. In Publication II we did WWW simulations where we implemented a more efficient version of the optimizations.

A switch move is a local perturbation and most strongly affects the system in its neighborhood. Before each trial step the system is in a minimum energy state and the force acting on each atom is zero. After the bonds have been switched, the only atoms which are affected by a non-zero force are the four atoms which have participated in the bond switch and their nearest neighbors. Therefore, in the first minimization step only these are moved (Fig. 3.3). In the next step the force is zero on all atoms except the ones which were moved during the last step and the atoms which interact with these atoms. Again, only the atoms with a non-zero force are moved. The minimized part is increased in this step wise fashion until any additional atoms would have a negligible effect. This gives a spherical selection comprising of the order of 1000 atoms, centered by the location of the original bond-switch. The minimization of this part continues after the growth

phase until the value of the potential energy has reached its minimum value or the early rejection rule is fulfilled.

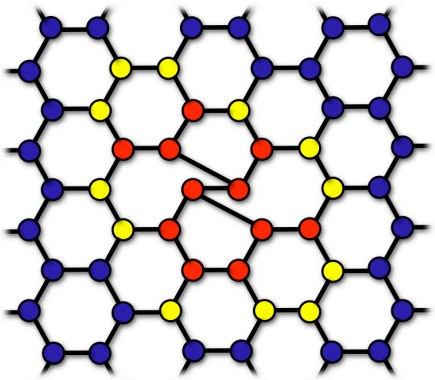

Figure 3.3: An illustration of how the fraction of atoms that are considered increases during minimization. The switch is seen as a z-shaped configuration of bonds. The atoms which are affected by this switch are red and are the ones minimized in the first step. The yellow atoms are included in the following minimization steps and in further minimization steps also blue atoms are considered.

If the system is minimized sufficiently so that the potential energy surface is nearly harmonic one can approximate the final energy of the system based on the total potential energy and total force at a certain step:

$$E_f \approx E_n - c|\mathbf{F_n}|^2, \tag{3.32}$$

where E_f is the final energy, E_n is the energy at CG step n, c is a constant and $\mathbf{F_n}$ is the total force of the system. If c is chosen conservatively, this equation can be used to estimate the final value of the minimization. Now the Metropolis acceptance rule of the MC method can be stated in a slightly different way. By solving Eq. (3.30) for E_f one can calculate a threshold energy

$$E_t = E(\Gamma_i) - k_B T \ln(r), \tag{3.33}$$

where r is a random number between 0 and 1. A trial step is accepted if the new potential energy, $E(\Gamma_j)$, is smaller than this threshold energy. One can now use the threshold energy and the approximation of the final energy to decide during the minimization if it should be stopped. Thus one can abort most minimizations early without a need to completely minimize structures which will not be accepted.

3.4 Minimization of atomistic systems

Publications II, IV and V study realistic 0 K structures of silica and twist GBs in Si. At 0 K the atoms occupy their minimum energy positions and so in these studies the quality of the results depends strongly on the minimization algorithm. Two kinds of minimizations have been employed, namely conjugate gradient minimization and simulated annealing.

3.4.1 Conjugate gradient method

The conjugate gradient (CG) method (Press et al., 1995) is an efficient iterative minimization algorithm. A local minimum of any scalar-valued function $E(\mathbf{x})$, where $\mathbf{x}$ is an N dimensional vector, can be found if its gradient $\nabla E(\mathbf{x})$ is known. It can be proven that quadratic functions are minimized in at most N steps. When an atomic system is minimized with respect to the positions of the atoms a minimum is in fact reached much faster. If the system is reasonably close to a local minimum then the number of steps needed to reach it is of the order of tens to hundreds of steps. Due to its basic approach the CG algorithm is usually not able to find the global minimum as it gets stuck in the local minimum energy state which is structurally most similar to the initial state. In the WWW method we employed this method to calculate the new structure after a bond-switch, since the post-switch state is close to the state prior to the switch.

Starting from some state $\mathbf{x}_0$ the solution is approached iteratively by updating the state with a gradient term denoted by $\mathbf{h_i}$ at each step i,

$$\mathbf{x}_{i+1} = \mathbf{x}_i + \alpha \mathbf{h_i}, \tag{3.34}$$

where $\mathbf{x}_i$ is the state $\mathbf{x}$ in the i:th iteration. The parameter α is obtained by minimizing $E(\mathbf{x}_i + \alpha \mathbf{h_i})$ with respect to α. This is a one dimensional minimization problem for which there is a number of powerful techniques (Press et al., 1995). The gradient term $\mathbf{h_i}$ is calculated as follows

$$\mathbf{h_0} = -\nabla E(\mathbf{x}_0) \tag{3.35}$$

$$\mathbf{h_i} = -\nabla E(\mathbf{x}_i) + \gamma \mathbf{h_{i-1}}. \tag{3.36}$$

where the constant γ can be calculated using the Polak-Ribiere method

$$\gamma = \frac{(\nabla E(\mathbf{x}_i) - \nabla E(\mathbf{x}_{i-1})) \cdot \nabla E(\mathbf{x}_i)}{\nabla E(\mathbf{x}_{i-1}) \cdot \nabla E(\mathbf{x}_{i-1})} \tag{3.37}$$

If γ is set to zero the CG method reduces to the steepest descent method.

3.4.2 Simulated annealing

When performing a minimization with simulated annealing the physical process of annealing solids is mimicked (van Laarhoven and Aarts, 1987). Annealing denotes a process in which the material is first heated up to a high temperature, followed by a slow cooling to 0 K. At the end of the anneal, the atoms will have arranged themselves in their minimum energy state. The reason for this self-organizing behavior is as follows. If a material has reached equilibrium at a certain temperature T, then the distribution of states is given by the Boltzmann distribution (Eq. 3.26). At high temperatures where the system is melted, almost all possible states are sampled. At low temperatures only a limited number of low energy states are sampled. If the anneal is sufficiently slow the material will be in equilibrium at each temperature, and as the temperature goes down towards 0 K, only the minimum energy state will have a finite probability at the end. If the cooling is too fast, then equilibrium is not reached at each temperature and the materials can become trapped in a metastable local minimum.

With simulated annealing almost any kind of a function can be minimized. Even though only atomistic systems have been studied in this work, also difficult combinatorial problems such as the travelling salesman problem can be solved with it. In general the algorithm is a MC simulation where the temperature is slowly reduced. In more detail it is as follows. First, a cost function to be minimized is defined. In our simulations the cost function is the potential energy of the system. Second, a set of possible trial steps that change the parameters of the cost function are defined. These steps should be local so that the new trial parameters are in some sense close to the previous ones. This allows the algorithm to iteratively improve the solution. Third, a criterion for accepting or rejecting a trial step is defined. Here a good choice is the Metropolis acceptance criterion (Eq. 3.30) since it allows the system to escape local minimums. Fourth, the simulation is performed. A starting point is created which is then iteratively improved by trial steps which are accepted or rejected according to the given criterion. The simulation starts at a high temperature and the temperature is slowly lowered so that the global minimum is found.

In this work simulated annealing is done by performing either WWW or MD simulation. When a melted material is annealed with the WWW method the final state is an amorphous solid. This is due to limited computational resources, with a much slower anneal the simulation would find the crystalline state. Simulated annealing can also be accomplished with a normal MD simulation. In a MD simulation the energy distribution is a Boltzmann distribution. Also, each iterative step in a MD simulation is a small local change of the state. In this regard the same arguments for the effectiveness of the algorithm apply. In addition, a MD simulation is a direct simulation of the physical anneal that we used as a model. The same limitations that apply for WWW anneals, also apply for MD anneals.

The crystalline global minimum is not in general found if the whole system was initially melted. If there is a crystalline seed which is not melted then this is not true as the crystalline seed acts as a site for crystallization. In our GB studies (Publications IV and V) the two crystalline grains acted as seeds for crystallization and as border conditions for the allowed configurations. This allowed us to find the ordered, crystalline GB structures.

Chapter 4

Analysis of simulation data

In this work structural analysis plays an important role. In Publications I-III amorphous structures are compared to experimental results to ensure that they are realistic. In Publications IV and V the structure of the GBs are studied to characterize how ordered they are and if there are structural units. In addition an order parameter is used to define which atoms were considered not to be crystalline.

A MC or MD simulation produces a series of atomistic structures as a function of time or a sequence of iteration steps. This huge amount of data needs to be characterized using various measures for it to be manageable. The first important tool is the visualization software that has been developed during the course of this work. It enables one to gain insight into the structures and processes in the systems under study. Other important measures are the radial distribution function (RDF), bond angle distributions and ring statistics, which can be used to characterize local order. Order parameters have been employed to automatically divide atoms into crystalline and non-crystalline atoms. Also, the volume and shape of contiguous patches of selected atoms have been calculated.

4.1 Radial distribution function

A good way to measure local structure is the radial distribution function (RDF), since it is experimentally measurable and provides an important tool for comparing the computationally created structures with the real ones. The density function $\rho(r)$ is defined to be the average number density of atoms at a distance r from any other atom. This function is zero at small r values as at small distances atoms experience a strong repulsion. In amorphous materials there is a sharp peak at the nearest neighbor distance, followed by broader peaks at the next nearest neighbor distance. For large r values the function is close to the average number density of atoms $\rho_0 = N/V$. In crystals, where there is long-ranged order, there are only sharp peaks. The reduced radial distribution function $G(r)$ is obtained from the

density function:

$$G(r) = 4\pi r(\rho(r) - \rho_0). \tag{4.1}$$

This is a function which oscillates around zero. Using X-ray diffraction one can measure the structure factor $S(k)$ and obtain $G(r)$ by doing a inverse Fourier transform of the reduced structure factor function $k(S(k) - 1)$.

The RDF is here defined as:

$$T(r) = 4\pi r\rho(r). \tag{4.2}$$

For silica where there is more than one element, the radial distribution function has to be weighted in order to directly compare to experimental neutron-diffraction measurements (Susman et al., 1991b,a).

4.2 Ring statistics

Another way of characterizing materials is to look at the distribution of rings. An irreducible ring is the shortest non-intersecting path along the bonds which goes from one neighbor of an atom to another neighbor of the same atom. If a ring is irreducible, then no two atoms in the ring are connected through a shorter path than the path along the ring. In silica, oxygen atoms are ignored and only the rings starting from Si atoms are calculated. Also when the length of a ring is calculated, only the number of Si atoms are counted. Ring statistics are useful for characterizing structural order. Crystalline Si and silica comprise only 6-fold rings while amorphous Si and silica have a wider distribution of ring sizes. Small rings, such as 4-fold rings in Si, are a sign of strained high energy structures.

In the WWW simulations the bond network is explicitly defined and so these are used to calculate the ring statistics. In MD simulations bonds can be defined to be between atoms which are within a certain distance from each other. Here the ring statistics are influenced by the chosen cutoff distance. Rings are calculated using a simple recursive algorithm. First all the atoms which are one bond away from C are compared to B, if any of those are B then the ring is threefold. If none of them is B then all the atoms that are two bonds away from C are compared to B. If one of those is B then the ring is fourfold. This is continued until the shortest rings are found.

4.3 Structural order parameters

In this work two structural order parameters are used to classify atoms as either being in a crystalline grain or a disordered region. In Publication III a position dependent order parameter is used to find the amorphous cluster while in Publications IV and V a bond orientational order parameter is used to find the GB atoms.

The latter order parameter is in general better than the one used in Publication III. It is not dependent on the rotation of the crystal, it transfers to different crystalline lattices, and it does not require a pre-defined reference lattice. Both order parameters need to know which atom are bonded. Two atoms are here defined to be bonded if they are within a certain distance of each other. This distance is the one where there is a minimum between the nearest and second-nearest neighbor peaks in the RDF. The classification results improve if the atom coordinates do not have contributions from thermal vibration. In Publication III thermal disorder is eliminated by calculating the order parameter only for systems quenched to 0 K using conjugate gradient minimization. In Publications IV and V time-averaged positions are used.

4.3.1 Position dependent order parameter

In Publication III a simple order parameter is used to classify atoms as either amorphous or crystalline. Atomic positions are compared with atomic sites of a reference Si crystal that extends throughout the supercell and coincides with the crystalline region surrounding the amorphous cluster. The order parameter p_i for atom i is given by

$$p_i = \Delta r_i - \frac{1}{n_i} \sum_{j \neq i} \Delta r_j, \tag{4.3}$$

where the summation goes over the n_i atoms within 2.7 Å of atom i and Δr_i is the smallest distance of atom i from a site of the reference crystal. The second term ensures that a rigid translation in any direction does not change the order parameter. The order parameter is zero for crystals that have the same density and orientation as the reference crystal. Amorphous regions and crystals with a different density or orientation give rise to a nonzero value in the mean. We define the crystalline part of the system to be the largest contiguous cluster of atoms where each atom has a value of p_i less than 0.5 Å. The rest of the system is then classified as amorphous. In this way atoms within the amorphous region having small values of p_i by chance are correctly classified as amorphous.

4.3.2 Bond orientational order parameter

In order to identify atoms in the GBs in Publications IV and V we use a bond orientational order parameter per atom (ten Wolde et al., 1995) which is able to classify local order in the neighborhood of an atom. In Fig. 4.1 we show the values of $q(i)$ for a relaxed $\Sigma 5$ boundary. It is seen that $q(i)$ rapidly approaches unity outside the GB region and that it has a mean value of about 0.4 within the GB. This is also typical for other relaxed GB structures. $q(i)$ is unity in a perfect crystal and tends to zero in a completely disordered solid.

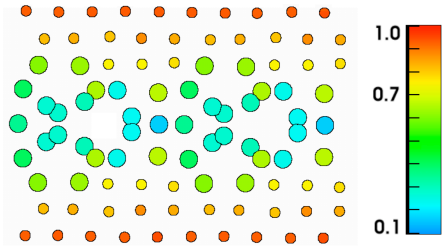

Figure 4.1: The variation of the order parameter $q(i)$ across a relaxed $\Sigma 5$ GB structure, viewed sideways along $\langle 310 \rangle$. Large (small) circles show atoms with $q(i) < 0.7$ ($q(i) > 0.7$). Atoms are colored in the online version according to the value of $q(i)$ as indicated by the color bar. (From Publication IV).

For each atom we calculate a set of complex numbers

$$q_{lm}(i) = \frac{1}{N_b(i)} \sum_{j=1}^{N_b(i)} Y_{lm}(\hat{\mathbf{r}}_{ij}), \tag{4.4}$$

where $N_b(i)$ is the number of neighbors of atom i, $Y_{lm}(\hat{\mathbf{r}}_{ij})$ are spherical harmonics and $\hat{\mathbf{r}}_{ij}$ is a unit vector from atom i to a neighbor j. From this we construct a complex vector $\mathbf{q}_l(i)$ which has $2l+1$ components proportional to $q_{lm}(i)$, and $\hat{\mathbf{q}}_l(i)$ which is a normalized $\mathbf{q}_l(i)$ vector. For atom i we then define the following order parameter:

$$q(i) = \frac{1}{N_b(i)} \sum_{j=1}^{N_b(i)} \hat{\mathbf{q}}_6(i) \cdot \hat{\mathbf{q}}_6^*(j). \tag{4.5}$$

In order to analyze what this order parameter measures Eq. 4.5 is first expressed in terms of $\mathbf{q}_6$

$$q(i) = \frac{1}{N_b(i)} \sum_{j=1}^{N_b(i)} \frac{\mathbf{q}_6(i) \cdot \mathbf{q}_6^*(j)}{\sqrt{\mathbf{q}_6(i) \cdot \mathbf{q}_6^*(i)}\sqrt{\mathbf{q}_6(j) \cdot \mathbf{q}_6^*(j)}}, \tag{4.6}$$

The dot term $\mathbf{q}_6(i) \cdot \mathbf{q}_6^*(j)$ is given by

$$\begin{aligned}
\mathbf{q}_6(i) \cdot \mathbf{q}_6^*(j) &= \sum_{m=-6}^{6} q_{6m}(i) q_{6m}^*(j), \\
&= \frac{1}{N_b(i) N_b(j)} \sum_{m=-6}^{6} \sum_{k=1}^{N_b(i)} \sum_{k'=1}^{N_b(j)} Y_{6m}(\hat{\mathbf{r}}_{ik}) Y_{6m}^*(\hat{\mathbf{r}}_{jk'}), \\
&= \frac{1}{N_b(i) N_b(j)} \sum_{k=1}^{N_b(i)} \sum_{k'=1}^{N_b(j)} \frac{13}{4\pi} P_6(\cos \gamma_{ik,jk'}),
\end{aligned} \tag{4.7}$$

where the addition theorem of spherical harmonics has been used in the last step. P_6 is the sixth order Legendre polynomial and $\gamma_{ik,jk'}$ is the angle between vectors $\hat{\mathbf{r}}_{ik}$ and $\hat{\mathbf{r}}_{jk'}$.

Inserting Eq. 4.7 into 4.6 gives

$$q(i) = \frac{1}{N_b(i)} \sum_{j=1}^{N_b(i)} \frac{\sum_{k=1}^{N_b(i)} \sum_{k'=1}^{N_b(j)} P_6(\cos \gamma_{ik,jk'})}{\sqrt{\sum_{k,k'} P_6(\cos \gamma_{ik,ik'})} \sqrt{\sum_{k,k'} P_6(\cos \gamma_{jk,jk'})}}. \tag{4.8}$$

This equation shows that $q(i)$ is always real. It is a measure of the correlation between the angular distribution of the bonds to atom i and the angular distribution of the bonds to i's neighbors.

4.4 Visualization

In computational science and engineering visualisation plays an increasingly important role. Visualization is often an efficient way of rapidly gaining insight into a problem. Combined with analysis tools visualizations can give also quantitative insight, in addition to the qualitative information that pure visualization gives. In this work a visualization and analysis package for atomistic simulations has been developed and it has been used to produce the illustrations in Publications III-V. Many important results, such as structural units in twist GBs, were first found by visual inspection. The visulization package is described in more detail in Appendix A.

Chapter 5

Overview of the results

This thesis comprises five publications and they are here presented in chronological order.

5.1 Heat transfer over an amorphous/crystalline interface in silicon

In Publication I we calculated the heat transfer over an interface between amorphous and crystalline Si near room temperature. The simulation supercell comprised a layer of amorphous Si between slabs of crystalline Si. Periodic boundary conditions were applied in all directions and thus the simulated system corresponded to an infinite superlattice with alternating slabs of amorphous and crystalline Si. Three systems of different sizes were studied to control finite-size effects. The crystalline slabs had a thickness of 187-296 Å and the amorphous part had a thickness of 38-100 Å.

The amorphous patch in the supercell was created using the WWW method. The RDF and bond-angle distribution of this patch showed that it was of good quality. The heat-transport problem was studied by doing a non-equilibrium MD simulation with the Stillinger-Weber potential model. By transporting kinetic energy from a "cool" region in a crystalline slab to a "hot" region in a neighboring crystalline slab, a temperature gradient was created over the system. In the amorphous and crystalline parts of the system the temperature profile was linear but had different slopes. The slope gives the thermal conductivity which can thus be measured separately in different parts of the system.

The measured thermal conductivity of the amorphous part was in agreement with previous theoretical and experimental data (Feldman et al., 1993). In the crystalline parts it was an order of magnitude smaller than the experimental value and was dependent on the size of the crystalline slab. We attributed this to finite-size effects, the mean free path of phonons which transport heat is of the order of

1000 Å in Si. Near room temperature the contribution from electrons to thermal conductivity is negligible (Shanks et al., 1963). We also noted that the interface did not show any thermal boundary resistance.

5.2 Improved potential model for amorphous silica

Publication II was motivated by the need to both develop an efficient implementation of the WWW method, and to improve its description of amorphous silica.

There exists at least six Keating-like potentials for silica and we implemented and tested all of them. We found that the structure of amorphous silica was not reproduced correctly by any of them. We recognized that their main deficiency was that the oxygen bond-angle distribution was not reproduced correctly, but was shifted towards smaller angles. To alleviate this problem we created a new set of potential model parameters where we strengthened the oxygen bond-bending term. Our improved potential model reproduces experimental data on the bond-angle distribution to oxygen atoms (Mozzi and Warren, 1969; Mauri et al., 2000) almost perfectly.

Comparing the radial distribution function with experimental data (Susman et al., 1991b) it was seen that the overall fit is improved using our potential model. This is most evident in the second peak which corresponds to the correlation between oxygen neighbors to the same Si atom. Also comparing the ring statistics in our model with previous MD simulations (Rino et al., 1993) we found that our potential model showed superior characteristics in that the fraction of small rings was lower than for the other potential models. The relative energies of free clusters comprising a two-, three- or four-membered ring calculated using our potential model match previous *ab-initio* results (Uchino et al., 2000) better than energies calculated using any other Keating-like potential model. The stiffer bond-bending term at oxygen atoms increased the energy of small rings leading to a more realistic distribution of rings.

In the supplementary material to the article details of the algorithmic improvements are presented. They are based on previously published optimizations of the WWW method (Barkema and Mousseau, 2000) and are here presented in section 3.3.1. In simulations comprising 1536 atoms the early rejection scheme speeds up the algorithm over 5 times compared to the standard WWW method. If also local minimization is used, the speed of the simulation is increased by more than factor of 35. These figures only give a rough estimate of the improvement in speed since the effectiveness of the optimization is dependent on the system size, temperature and on which optimization parameters are selected. In larger systems the speed up is even greater as global minimizations are avoided.

5.3 Stability of spherical amorphous clusters

In Publication III we have studied the crystallization dynamics of small clusters of amorphous Si embedded in crystalline Si. The stability of amorphous clusters is of interest in the case of phase-change memory devices where they are used to store information. Although Si is not used in such devices we used it here as our motivation for this work was to develop a methodology to investigate the stability of such clusters.

The initial computational supercell comprised a spherical region of amorphous Si with a radius of ≈27 Å, embedded in crystalline Si. The amorphous cluster was created separately by preparing a well-equilibrated amorphous supercell and cutting out a spherical region. This was then inserted into a spherical void created in crystalline Si. Melting and annealing a spherical region in crystalline Si would necessitate very high annealing rates to avoid complete recrystallization, leading to the formation of a high-energy disordered structure. The small clusters we simulated were used as models for more realistically sized clusters with a radius of ≈100 nm consisting of well-equilibrated amorphous Si.

By assuming the mobility of the interface follows an Arrhenius-like behavior, the radius r as a function of time t can be modeled by the following equation,

$$r(t) = r(0) - v_0 t \exp\left(-\frac{E}{kT}\right) - \rho \ln\left(\frac{\rho + r(0)}{\rho + r(t)}\right), \tag{5.1}$$

where E is the activation energy of the crystallization process, T is the temperature and $\rho = 2\sigma/\Delta E_v$. σ is the interface energy of the amorphous/crystalline interface and E_V is the excess internal energy of amorphous Si compared to crystalline Si. By doing a number of constant-temperature simulations (T=700 - 1500 K) we calculated parameters which enabled us to extrapolate the behavior of much larger clusters. First, the r dependence of the 0 K potential energy of the systems yielded $\Delta E_v = 1.19 \pm 0.27$ GJ/m^3 and $\sigma = 1010 \pm 200$ mJ/m^2. Second, the activation energy was obtained from the crystallization rate as a function of temperature. At temperatures below (above) 1150 K the activation energy was 0.73 ± 0.04 eV (1.52 ± 0.07 eV), indicating a change of mechanism at 1150K. After careful investigation we failed to find a reason for this change in behavior. Simulations of larger clusters at $T > 1150$ K, and longer simulations than we were able to do at $T < 1150$ K might shed a light on this problem. The radius of a theoretical 100 nm cluster would at room-temperature shrink by 10% in 11 minutes, which is not in total agreement with experiments (Ruault et al., 1984).

5.4 Twist grain boundaries in silicon

The main motivation for our work in Publications IV and V was to address the question of what is the intrinsic structure of twist GBs in Si. As discussed in section 2.4.2 there is contradicting evidence in the literature as to whether it is amorphous or ordered. In Publication IV we gave a detailed exposition of the $\Sigma 5$ twist GB and showed that it was ordered. The results were confirmed by minimizing the structures further with first principles methods thus validating the structures and the applicability of the Tersoff potential model for this problem. In Publication V we built on the previous article and presented results for the $\Sigma 25$, $\Sigma 13$, $\Sigma 17$, $\Sigma 5$ and $\Sigma 29$ (001) twist boundaries.

5.4.1 Computational approach

Our computational approach consisted of creating initial boundary structures which were thereafter slowly annealed with MD simulations. We recognized that previous computational studies had a number of limitations which reduced the phase space they were able to cover. First, changing the atomic density at the interface generates new structures which are not accessible to molecular dynamics (MD) simulation with a constant number of atoms. Second, by allowing the grains to slide with respect to each other all translational degrees of freedom are explored during annealing. Third, advancements in computer speed makes it possible to run orders of magnitude longer simulations that are required for sufficiently slow anneals.

The supercell comprised an integer number of CSL cells parallel to the boundary and 30 Å thick slabs of crystalline Si on either side. The supercell was periodic parallel to the boundary and had free surfaces perpendicular to the interface. This configuration allowed the two grains to slide with respect to each other easily. An alternative configuration would have had two GBs and periodic boundary conditions in all directions. This would have coupled the translational state of both boundaries and thus risked pinning it. The number of atoms per atomic layer in each CSL cell is $\nu = 25, 13, 17, 5$ and 29 for the $\Sigma 25$, $\Sigma 13$, $\Sigma 17$, $\Sigma 5$ and $\Sigma 29$ boundaries, respectively. ΔN denotes the number of atoms per primitive cell that were on random removed from the vicinity of the boundary. After sufficient annealing $\Delta N = 2\nu$ is equivalent to removing two entire (004) layers, which recreates the relaxed structure of $\Delta N = 0$. Hence removing 2ν or more atoms should not, in principle, create any new configurations. For each Σ boundary we created initial configurations for each unique atomic density in order to find the minimum energy structure. After the atoms had been removed from the boundary the boundary region was melted by doing a short MD simulation (100 ps) in that region using the Tersoff III (TS) potential (Tersoff, 1988a) . This removed all memory of the initial non-realistic structure at the interface.

The subsequent MD simulations annealed the system from 2000 K with a rate of 33 K/ns. We followed the evolution of the GB structure by averaging the positions of atoms over a time interval of 300 fs. This averaging removed most of the influence of thermal vibrations on atomic positions. The averaged configurations generated throughout each simulation were sampled every 100 ps and were the starting points of energy minimization to 0 K using the CG method. By calculating the GB energy of each relaxed structure we identified the minimum energy structure of the boundary.

In order to identify atoms in the GB we used a bond orientational order parameter per atom (ten Wolde et al., 1995). This criterion was used to evaluate the GB width and the standard deviations of bond lengths and angles.

5.4.2 Results

We calculated minimum energy structures comprising one primitive cell for all possible ΔN values for each boundary. This thorough and systematic study allowed us to find the true minimum energy structures for each boundary. In Fig. 5.1 we have plotted the energy of each boundary as a function of ΔN normalized by ν. The GB energy for each boundary depends strongly on ΔN. This shows the importance of sampling different values of ΔN, none of the boundaries having their minimum energy state at this value. The minimum energy structures were found for ΔN=47,21,32,7 and 47 for the $\Sigma 25$, $\Sigma 13$, $\Sigma 17$, $\Sigma 5$ and $\Sigma 29$ boundaries, respectively. The minimum energy increased with misorientation having a value of 836 mJ/m^2 for $\Sigma 25$ and 1108 mJ/m^2 for $\Sigma 29$.

The minimum energy structures of $\Sigma 25$, $\Sigma 13$ and $\Sigma 5$ are depicted in Fig. 5.2. $\Sigma 25$ has the lowest misorientation and a screw dislocation network can be clearly seen. In the intersections there are two different structural units which are here called A and B. In Fig. 5.3 these are presented in more detail. Also the $\Sigma 13$ and $\Sigma 5$ boundaries are seen to be formed by the same two structural units. In the case of $\Sigma 13$ all intersection comprise A units while in the case of $\Sigma 5$ both A and B units are present. As the misorientation increases the separation of the structural units decreases and in the case of $\Sigma 5$ the units actually touch. The fact that these boundaries are formed of structural units show clearly that these structures are ordered. The minimum energy structures of $\Sigma 17$ and $\Sigma 29$ are depicted in Fig. 5.4. There is no screw dislocation network in these boundaries, but there is still clear evidence of order. First, both boundaries have point group symmetry. It is $p2_1$ and $p2$ for the $\Sigma 17$ and $\Sigma 29$ boundaries, respectively. Second, the width of the bond-angle distribution is lower than for well equilibrated amorphous Si which is a sign of less structural disorder. Third, in the $\Sigma 29$ boundary structural units are visible. Also, there are no coordination defects in the $\Sigma 17$ boundary. In addition to the minimum energy structures there are also several other low energy ordered structures for each boundary which are presented in more detail in Publication V.

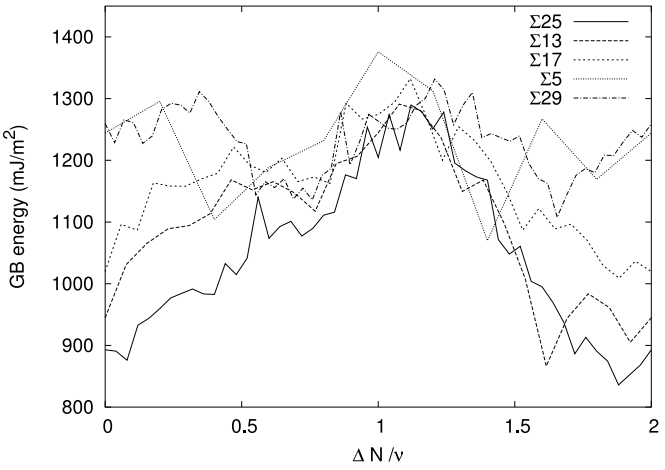

Figure 5.1: GB energy obtained with the TS potential as a function of the number, ΔN, of atoms removed normalized by the number, ν, of atoms in each layer parallel to the GB contained in one primitive cell of the GB.

Increasing the size of the supercell allows the system to adopt new structures. The reason is two-fold: first, there are more possible ΔN values since removing up to two complete atomic layers introduces new structures; second, boundary structures with periodicity larger than one primitive cell are possible. For equal ΔN values the minimum energy structure should be equal as long as the structure periodicity is not larger than the simulated supercell. We studied some supercells comprising 2×2 and 4×4 primitive cells but did not do a thorough investigation of all possible boundaries due to finite computational resources. Simulating $\Sigma 5$ structures with $\Delta N = 7$ in supercells comprising 2×2 primitive cells revealed several new higher-energy metastable structures which were also composed of A and B units (Fig. 5.5). At temperatures above 0 K the $\Sigma 5$ boundary can visit these metastable states as only limited structural reconfiguration is required. In the case of $\Sigma 13$ we found a similar phenomenon when looking at the minimum energy structures for ΔN=21-25 (Fig. 5.6). These boundaries have identical structures except that the fraction of A and B units at the intersections is different. When ΔN increases, the fraction of A units goes down while the boundary energy goes up. These results in 2×2 supercells again show the robustness of the structural units and can also be used to infer the structure of even bigger boundaries.

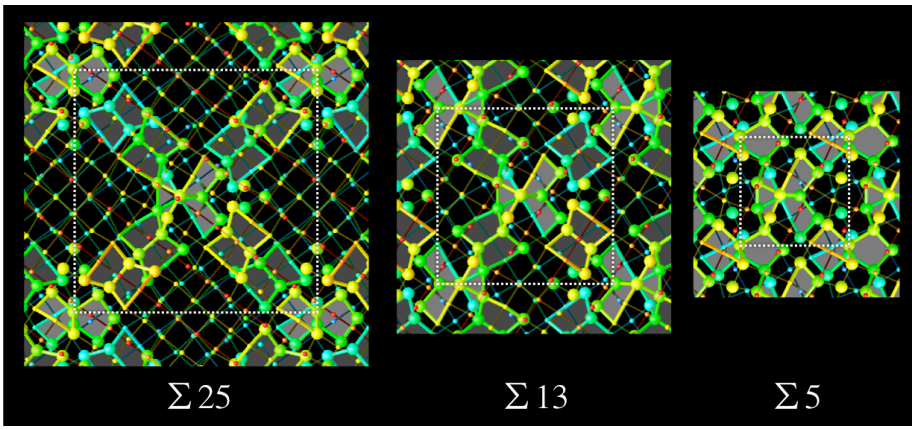

Figure 5.2: Plane views of minimum energy $\Sigma 25, \Sigma 13$ and $\Sigma 5$ boundaries. All figures have identical scale. The coloring of atoms and bonds indicates the position perpendicular to the boundary, blue (red) atoms or bonds are further from (closer to) the viewer. The larger atoms are defined to be in the GB and the thicker bonds are bonds forming five-membered rings. We have indicated structural units in the plane view by shading the 5 membered rings within them. Structural units in the cores of screw dislocation are shaded darker gray and A and B units at the screw dislocation intersections are shaded lighter gray.

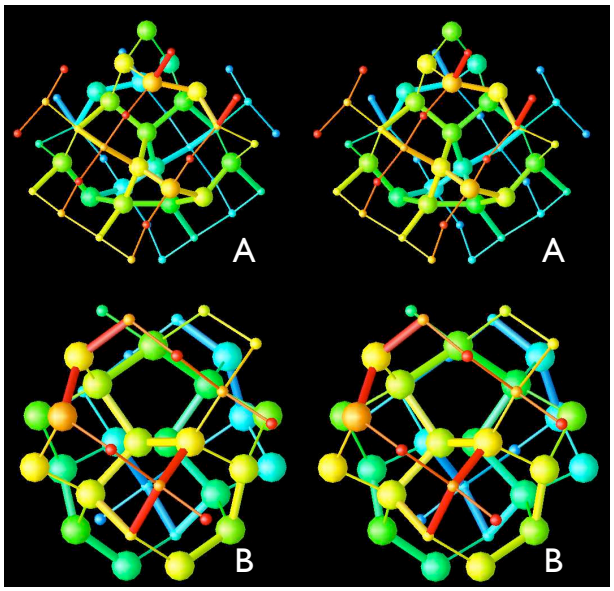

Figure 5.3: Stereopairs of the two structural units. The one on the top is called A while the lower one is called B. See caption to Fig. 5.2.

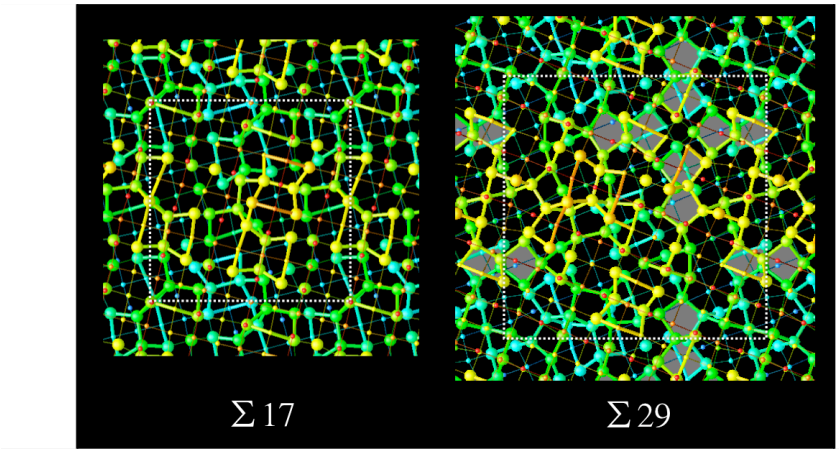

Figure 5.4: Plane views of minimum energy Σ17 and Σ29 boundaries. The figures have identical scale to the ones in Fig. 5.2. See caption to Fig. 5.2

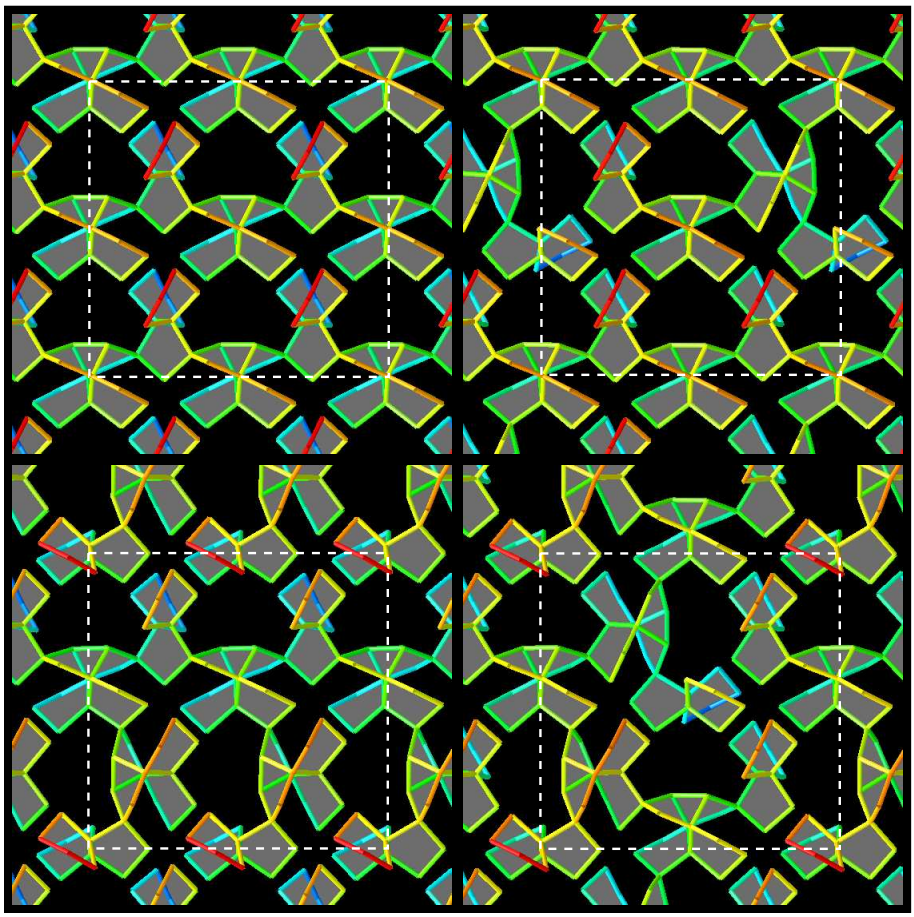

Figure 5.5: $\Sigma 5$ boundaries where each computational supercell contained 2×2 primitive cells in the GB plane. In each case the number of atoms removed per primitive cell is $\Delta N = 7$. The boundary energies are 1069, 1091, 1095 and 1121 mJ/m^2 for the top left, top right, bottom left and bottom right configurations, respectively. The size of the 2×2 supercell is indicated by a white dashed box. Bonds in five-membered rings are shown to highlight the structural units. See caption to Fig. 5.2. Reprinted with permission from Publication V. Copyright (2006) by the American Physical Society.

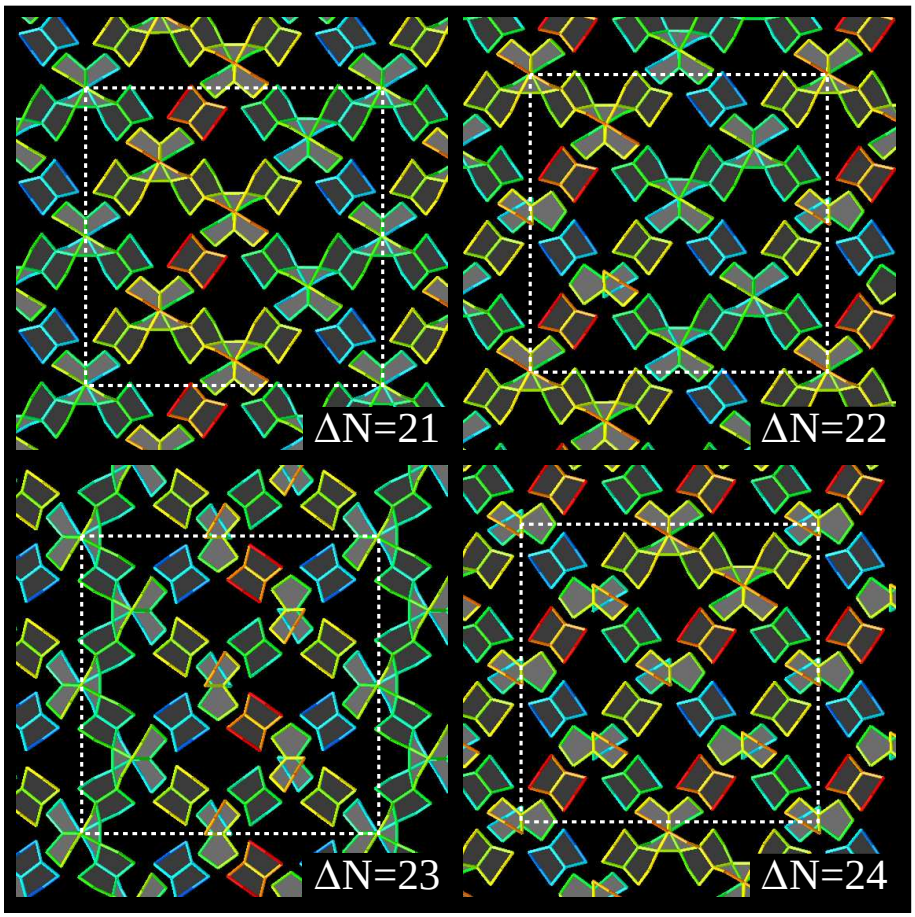

Figure 5.6: $\Sigma 13$ boundaries where each simulation supercell contained 2×2 primitive cells in the GB plane. In each case the value of ΔN signifies the number of atoms removed per primitive cell. The size of the supercell is indicated by white dashed boxes. Bonds in five-membered rings are shown to highlight the structural units. See caption to Fig. 5.2. Reprinted with permission from Publication V. Copyright (2006) by the American Physical Society.

Chapter 6

Summary

In this thesis the structure and kinetics of a number of silicon and silica systems have been studied with computer simulations. The author has developed independently all simulational and analysis tools used in these studies. This has been vital in order to find novel ways to simulate, and in particular analyze the studied systems. The research itself has been published in five publications, all of which are included in this compilation. The main results of this thesis are as follows. First, new potential model parameters which can be used for creating realistic amorphous silica have been developed. Second, the collapse of an amorphous cluster embedded in crystalline silicon has been modeled. The methodology can also be used for other materials more relevant to phase change memory devices. Third, new ordered structures have been found for twist grain boundaries in silicon by considering all possible atomic densities at the boundary. In addition to order, structural units were also found. These formed a number of boundaries as is predicted by the structural unit model. This is perhaps the most significant contribution in this thesis as the question whether high-angle twist grain boundaries are formed of amorphous intergranular films has been an actively disputed topic in the grain boundary community.

The next topic of research also concerns grain boundaries. Now that ordered low energy grain boundary structures at 0 K have been calculated, the focus will change to their properties at finite temperatures. When grain boundaries are heated, the boundary undergoes a melting transition at temperatures lower than the bulk melting temperature. The preliminary results show that this is a continuous transition. They also show that the structural units are very stable. At temperatures up to 80% of the melting temperature the network of structural units in $\Sigma 25, \Sigma 13$ and $\Sigma 5$ is stable, but visits also the higher energy metastable states presented in the case of $\Sigma 5$. At temperatures above this, there are still metastable structural units, even though most of the boundary has melted.

Appendix A

Atomicdx

The visualization package that the author has developed is named Atomicdx. It can visualize atoms and bonds, and also perform some simple analysis tasks. The main goal has been to develop a tool with which one can perform a visual examination of a series of atomistic systems (frames). This enables one to explore the system interactively and examine both its structure and the relationship between data associated with either atoms or bonds as a function of time. The structure of a frame is studied by drawing a selected set of atoms and bonds. The selection can be based on any atom or bond data. This enables one to draw only the interesting parts of a system. For example, in Publications IV and V the GB structure is easier to grasp if the crystalline grains are not drawn. Data associated with atoms or bonds are visualized by either changing the coloring, or the sizes or shapes of them based on the data. The data are usually scalar valued but for atoms one can also have vectorial data. Typical atom data are their potential, atom-type and velocity while typical bond data are the length of the bond, and atom data interpolated on the bonds.

Atomicdx has been implemented using Opendx (*www.opendx.org*). Opendx is an opensource visualization package that can be used to create visualizations of different kinds of data. The visualization is built as a network of data processing modules. The first module in the network imports data. The data are then passed on to modules which transform them in to a form that can be visualized. The visualization data are passed on to output modules which plot a graph, draw an image or write out data to a file. As Opendx has efficient data-caching only the parts of the network with changed input data will be executed. This allows even very large visualization networks to show good performance, but also means that the memory requirements can be relatively high. Atomicdx is built as such a network containing a number of custom modules to facilitate the loading of atomic systems and calculating certain data values useful for analysis and visualization. The goal of Atomicdx was to create a visualization tool that can be used with

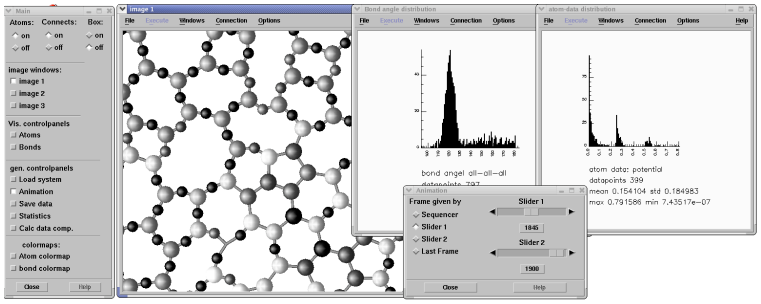

Figure A.1: A typical session in Atomicdx. The main control panel allows one to open the other control panels, images and colormaps and to choose which glyphs are visualized. Also a visualization and two data distributions is shown.

no prior knowledge of Opendx. Atomicdx can be operated with control panels having no need to touch the network itself. This hides the complexity of Opendx from the user but at the same time one can use the full power of Opendx within the created framework if needed. In Fig. A.1 an example of using Atomicdx is given showing two control panels and a visualization together with some statistics.

One can load atomistic systems into Atomicdx by reading in files which give the positions of the atoms and optionally also two scalars, a data vector, and bonding information. If there is no bonding information Atomicdx can calculate it using the cell-method (Frenkel et al., 2001). After the frames have been successfully loaded one can calculate new data for the bonds and atoms. These data are always calculated only for the active frame, not all frames. *Change* data are vectorial data associated with the atoms that measure the distance the atoms have moved between frames. If the number of atoms is different this is calculated only for the atoms that are in both frames. The identity of an atom is given by its index number, i.e. the order in which it appears in the input. It is useful for finding changes in structure between frames and also for looking at diffusion. One can also clusterize data and calculate a *cluster* data component. A cluster consists of a contiguous set of atoms which have a datavalue within a certain interval. In figure A.2 an example of clusterization is given. In the figure Si atoms have been clusterized by clusterizing the *type* data. One can also calculate *datadistance* data. These data allow us to classify atoms based on their distance from a set of atoms. The distance value for each atom is defined as the minimum number of bonds one has to traverse to get to the selected set. In figure A.2 an example of the datadistance is given. There the set of atoms from which the distance is calculated are the ones which form the previously mentioned clusters. Finally one can also calculate an atom dependent *custom* data component by writing an arithmetic expression involving any of the other data components.

The visualization capabilities in more detail are the following. Data are used

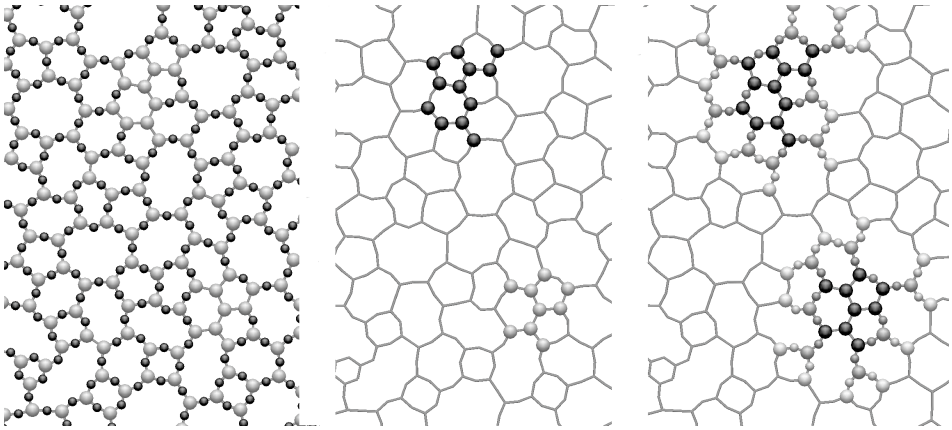

Figure A.2: Three visualization of a 2D-model of SiO illustrating the clusterization and data distance. *On the left:* Colors represent the type of atom. *Center:* Colors represent clusters of Si. Only the two largest ones are shown. *On the right:* Colors represent the datadistance from the clusters. Only the first four layers are drawn.

to set the color, size and shape of glyphs representing atoms and bonds. The coloring can also be affected by changing the color maps which map data values to colors. The glyph type depends on the chosen glyph data. Bonds are always drawn as tubes connecting the atoms. Atoms are drawn as spheres when the glyph-data are scalar and as arrows when the glyph data are vectorial. The radius of the sphere is proportional to the scalar value, and the arrow is in the direction of the vector with a length proportional to the length of the vector. One can change the amount of detail in the spheres and bonds to either produce output quality images by increasing it, or to produce fast visualizations with a fast refresh rate by decreasing it. The visualized system can be arbitrarily and interactively rotated and moved. It is also easy to zoom in on the interesting parts.

In the program one can analyze atom and bond data. Only the atoms and bonds selected to be shown in the visualization are included in the analysis, and the data that are analyzed are the one used for coloring. For both the atom and bond data one can calculate a histogram and other basic statistics such as minimum, maximum, mean and variance. One can also plot the atom data with respect to another user defined data as a scatter or line plot. In the line plot the value of the line is given by the mean, standard deviation, maximum or minimum of the coloring data. Other statistics include the bond-angle distribution and the radial distribution function.

References

Allen, M. P. and Tildesley, D. J. (1987). *Computer simulation of liquids*. Clarendon Press, New York, NY, USA.

Andersen, H. C. (1980). Molecular dynamics at constant pressure and/or temperature. *Journal of Chemical Physics*, 72:2384.

Ashcroft, N. W. and Mermin, N. D. (1976). *Solid State Physics*. Saunder Collage Publishing.

Balamane, H., Halicioglu, T., and Tiller, W. (1992). Comparative study of silicon empirical interatomic potentials. *Physical Review B*, 46:2250.

Barkema, G. and Mousseau, N. (2000). High-quality continuous random networks. *Physical Review B*, 62:4985.

Berendsen, H. J. C., Postma, J. P. M., van Gunsteren, W. F., DiNola, A., and Haak, J. R. (1984). Molecular dynamics with coupling to an external bath. *J. Chem. Phys.*, 81(8):3684–3690.

Brotherton, S. D. (1995). Polycrystalline silicon thin film transistors. *Semicond. Sci. Technol.*, 10:721–738.

Burlakov, V. M., Briggs, G. A. D., Sutton, A. P., and Tsukahara, Y. (2001). Monte carlo simulation of growth of porous SiO_x by vapor deposition. *Physical Review Letters*, 86:3052.

Chan, S. L. and Elliot, S. R. (1992). Calculation of diffusion activation energies in covalent solids: application to vitreous silica. *Journal of Physics: Condensed Matter*, 4:1269.

Cleri, F., Keblinski, P., Colombo, L., Phillpot, S. R., and Wolf, D. (1998). Correlation between atomic structure and localized gap states in silicon grain boundaries. *Phys. Rev. B*, 57:6247.

Cook, S. J. and Clancy, P. (1993). Comparison of semi-empirical potential functions for silicon and germanium. *Phys. Rev. B*, 47(13):7686–7699.

D'Anterroches, C. and Bourret, A. (1984). Atomic structure of (011) and (001) near-coincident tilt boundaries in germanium and silicon. *Phil. Mag. A*, 49:783.

Feldman, J. L., Kluge, M. D., Allen, P. B., and Wooten, F. (1993). Thermal conductivity and localization in glasses: Numerical study of a model of amorphous silicon. *Phys. Rev. B*, 48(17):12589–12602.

Frenkel, D., Frenkel, D., and Smit, B. (2001). *Understanding Molecular Simulation*. Academic Press, Inc., Orlando, FL, USA.

Gibson, J. B., Goland, A. N., Milgram, M., and Vineyard, G. H. (1960). Dynamics of radiation damage. *Phys. Rev.*, 120(4):1229–1253.

Grovenor, C. R. M. (1985). Grain boundaries in semiconductors. *J. Phys. C: Solid State Phys.*, 18:4079–4119.

Hedler, A., Klaumünzer, S. L., and Wesch, W. (2004). Amorphous silicon exhibits a glass transition. *Nature mat.*, 3:804.

Howe, J. M. (1997). *Interfaces in Materials*. John wiley sons, inc.

Justo, J. F., Bazant, M. Z., Kaxiras, E., Bulatov, V. V., and Yip, S. (1998). Interatomic potentials for silicon defects and disordered phases. *Physical Review B*, 58:2539.

Keating, P. (1966). Effect of invariance requirements on the elastic strain energy of crystals with application to the diamond structure. *Physical Review*, 145:637.

Keblinski, P., Phillpot, S. R., and Wolf, D. (1997). On the thermodynamic stability of amorphous intergranular films in covalent materials. *J. Am. Ceram. Soc.*, 80:177.

Keblinski, P., Phillpot, S. R., Wolf, D., and Gleiter, H. (1996). Thermodynamic criterion for the stability of amorphous intergranular films in covalent materials. *Phys. Rev. Lett.*, 77:2965.

Keskar, N. R. and Chelikowsky, J. R. (1992). Structural properties of nine silica polymorphs. *Physical Review B*, 46:1.

Kleinman, D. A. and Spitzer, W. G. (1962). Theory of the optical properties of quartz in the infrared. *Phys. Rev.*, 125(1):16–30.

Kohyama, M. and Yamamoto, R. (1994). Tight-binding study of grain boundaries in Si: Energies and atomic structures of twist grain boundaries. *Phys. Rev. B.*, 49:17102.

Kohyama, M., Yamamoto, R., Ebata, Y., and Kinoshita, M. (1988). The atomic and electronic structure of a <001> tilt grain boundary in Si. *J. Phys. C: Solid State Phys.*, 21:3205.

Mauri, F., Pasquarello, A., Pfrommer, B. G., Yoon, Y.-G., and Louie, S. G. (2000). Si-O-Si bond-angle distribution in vitreous silica from first principles Si NMR analysis. *Phys. Rev. B*, 62:4786.

Metropolis, N., Rosenbluth, A. W., Rosenbluth, M. N., Teller, A. H., and Teller, E. (1953). Equation of state calculations by fast computing machines. *The Journal of Chemical Physics*, 21(6):1087–1092.

Morigaki, K. (1999). *Physics of Amorphous Semiconductors*. Imperial College Press.

Mozzi, R. L. and Warren, B. E. (1969). The structure of vitrous silica. *J. Appl. Crystallogr.*, 2:164.

Nosé, S. (1984). A unified formulation of the constant temperature molecular dynamics method. *J. Chem. Phys.*, 81:511.

Otsuki, A. (2001). Misorientation dependence of energies of Si(001) twist grain boundaries. *Interf. Sci.*, 9:293.

Payne, M. C., Bristowe, P. D., and Joannopoulos, J. D. (1987). Ab initio determination of the structure of a grain boundary by simulated quenching. *Phys. Rev. Lett.*, 58:1348.

Press, W. H., Teukolsky, S. A., Wtterling, W. T., and Flannery, B. P. (1995). *Numerical Recipies in C*. Cambridge University Press.

Read, W. T. and Shockley, W. (1950). Dislocation models of crystal grain boundaries. *Phys. Rev.*, 78:275.

Rino, J. P., Ebbsjö, I., Kalia, R. K., Nakano, A., and Vashishta, P. (1993). Structure of rings in vitreous SiO_2. *Physical Review B*, 47(6):3053.

Ruault, M. O., Chaumont, J., Penisson, J. M., and Burret, A. (1984). High resolution and in situ investigation of defects in Bi-irradiated Si. *Phil. Mag. A*, 50:667–675.

Shanks, H. R., Maycock, P. D., Sidles, P. H., and Danielson, G. C. (1963). Thermal conductivity of silicon from 300 to 1400°K. *Phys. Rev.*, 130(5):1743–1748.

Stillinger, F. H. and Weber, T. A. (1985). Computer simulation of local order in condensed phases of silicon. *Phys. Rev. B*, 31:5262.

Streitz, F. H., Glosli, J. N., and Patel, M. V. (2006). Beyond finite-size scaling in solidification simulations. *Phys. Rev. Lett.*, 96(22):225701.

Susman, S., Volin, K. J., Montague, D., and Price, D. L. (1991a). Temperature dependance of the first sharp diffraction peak in vitreous silica. *Phys. Rev. B*, 43:11076.

Susman, S., Volin, K. J., Price, D. L., Grimsditch, M., Rino, J. P., and Kalia, R. K. (1991b). Intermediate-range order in permanently densified vitrous SiO_2: A neutron diffraction and molecular dynamics study. *Phys. Rev. B*, 43:1194.

Sutton, A. (1991). Grain boundaries in elemental and compound semiconductors. In Werner, J. and Strunk, H., editors, *Polycrystalline Seiconductors II, Springer Proc. Phys.*, page 116. Springer-verlag: Berlin.

Sutton, A. P. and Balluffi, R. W. (1995). *Interfaces in crystalline materials*. Oxford University Press, New York.

Sutton, A. P. and Vitek, V. (1983). On the structure of tilt grain boundaries in cubic metals. I. Symmetrical tilt boundaries. *Phil. Trans. Soc. Lond. A*, 309:1.

Tarnow, E., Dallot, P., Bristowe, P. D., Joannopoulos, J. D., Francis, G. P., and Payne, M. C. (1990). Structural complexity in grain boundaries with covalent bonding. *Phys. Rev. B*, 42:3644.

ten Wolde, P. R., Ruiz-Montero, M. J., and Frenkel, D. (1995). Numerical evidence for bcc ordering at the surface of a critical fcc nucleus. *Phys. Rev. Lett.*, 75:2714.

Tersoff, J. (1986). New empirical model for the structural properties of silicon. *Physical Review Letters*, 56:632.

Tersoff, J. (1988a). Empirical interatomic potential for silicon with improved elastic properties. *Phys. Rev. B*, 38:9902.

Tersoff, J. (1988b). New empirical approach for the structure and energy of covalent systems. *Physical Review B*, 37:6991.

Tsuneyuki, S., Tsukada, M., Aoki, H., and Matsui, Y. (1988). First-principles interatomic potential of silica applied to molecular dynamics. *Phys. Rev. Lett.*, 61(7):869–872.

Tu, Y. and Tersoff, J. (2000). Structure and energetics of the Si-SiO_2 interface. *Physical Review Letters*, 84(19):4393.

Tu, Y., Tersoff, J., and Grinstein, G. (1998). Properties of continuous-random-network model for amorphous systems. *Physical Review Letters*, 81:4899.

Uchino, T., Kitagawa, Y., and Yoko, T. (2000). Structure, energies and vibrational properties of silica rings in SiO_2 glass. *Phys. Rev. B*, 61:234.

van Beest, B. W. H., Kramer, G. J., and van Santen, R. A. (1990). Force fields for silicas and aluminophosphates based on ab initio calculations. *Phys. Rev. Lett.*, 64(16):1955–1958.

van Laarhoven, P. J. M. and Aarts, E. H. L. (1987). *Simulated Annealing: Theory and Applications*. D. Reidel Publishing Company.

Vashishta, P., Kalia, R. K., Rino, J. P., and Ebbsjö, I. (1990). Interaction potential for sio_2: A molecular-dynamics study of structural correlations. *Phys. Rev. B*, 41(17):12197–12209.

Vink, R., Barkema, G., van der Weg, W., and Mousseau, N. (2001). Fitting the Stillinger-Weber potential to amorphous silicon. *Journal of non-crystalline solids*, 282:248.

Wang, Z. Q., Dregia, S. A., and Stroud, D. (1994). Energy-minimization studies of twist grain boundaries in diamond. *Phys. Rev. B.*, 49:8206.

Wooten, F., Winer, K., and Weaire, D. (1985). Computer generation of structural models of amorphous Si and Ge. *Physical Review Letters*, 54:1392.